Université d'Ottawa · University of Ottawa

Université d'Ottawa · University of Ottawa

FACULTÉ DES ÉTUDES SUPÉRIEURES ET POSTDOCTORALES

FACULTY OF GRADUATE AND POSTDOCTORAL STUDIES

ZENG, Fei

AUTEUR DE LA THÈSE - AUTHOR OF THESIS

M.A.Sc. (Electrical Engineering)

GRADE - DEGREE

School of Information Technology and Engineering

FACULTÉ, ÉCOLE, DÉPARTEMENT - FACULTY, SCHOOL, DEPARTMENT

TITRE DE LA THÈSE - TITLE OF THE THESIS

Synthesis and Realization of Fiber Bragg Grating Based All-Optical Microwave Filters

Jianping Yao

DIRECTEUR DE LA THÈSE - THESIS SUPERVISOR

EXAMINATEURS DE LA THÈSE - THESIS EXAMINERS

Pierre Berini

Langis Roy

J.-M. De Koninck, Ph.D.

LE DOYEN DE LA FACULTÉ DES ÉTUDES SUPÉRIEURES ET POSTDOCTORALES

SIGNATURE

DEAN OF THE FACULTY OF GRADUATE AND POSTDOCTORAL STUDIES

Synthesis and Realization of Fiber Bragg Grating Based All-Optical Microwave Filters

By

Fei Zeng

A thesis submitted in partial
fulfillment of the requirements for
the degree of

Master of Applied Science

Ottawa-Carleton Institute of Electrical and Computer Engineering
School of Information Technology and Engineering
Faculty of Engineering
University of Ottawa

September 2003

Your file Votre référence
ISBN: 0-612-90366-4
Our file Notre référence
ISBN: 0-612-90366-4

ABSTRACT

Synthesis and implementation of a fiber Bragg grating (FBG) based all-optical microwave filter are presented in this thesis. The all-optical microwave filter is synthesized using genetic algorithms, and is implemented using fiber Bragg gratings, and other photonic components.

To design an FBG-based all-optical microwave filter with given specifications, the tapping coefficients (or the reflectivities of the FBGs) and tapping intervals should be carefully determined. Standard digital filter design algorithms cannot be applied readily to all-optical microwave filter synthesis; because incoherent interference prevents the inclusion of negative coefficients. In this thesis, genetic algorithm (GA) is applied to the optimum design of finite impulse response (FIR) filters. As numerical techniques from nature evolution, genetic algorithms are well suited for simultaneous optimization of multivariable problems and can also be used to find families of solutions.

To implement the FBG-based all-optical microwave filters, some practical issues must be addressed carefully. First, it is difficult to fabricate an FBG with peak reflectivity less than 0.1. With genetic algorithms, one may simply

specify a low bound to the reflectivity and this problem can be solved easily. Another important fact is that the power spectrum of the modulated broadband light is not as flat as we expect, using an un-flat light source will lead to a microwave filter with poorer performance. To solve this problem, in the algorithms a variable is introduced to calibrate the filter coefficients according to the power spectrum of the incident light.

Experiments are carried out using two FBG arrays with the reflectivities obtained using the genetic algorithms. It is found that the experimental results agree well with the theoretical results if the filter coefficients are calibrated by considering both the un-flat power spectrum of the light source and the power reflectivities of the FBGs.

Finally, discussion on the dispersion effects on the performance of the FBG-based microwave filters is provided. We find that the effective coefficients for all-optical microwave filter vary with the modulating frequency and the FBG synthesis parameters. The coefficient errors caused by the dispersion can be significantly reduced by carefully choosing FBGs with short length and small reflectivities.

TABLE OF CONTENTS

LIST OF FIGURES

Number *Page*

LIST OF TABLES

Number *Page*

ACKNOWLEDGMENTS

I owe a deep sense of gratitude to my advisor, Dr. Jianping Yao. He has been a source of constant encouragement and enthusiasm. I thank him for providing valuable suggestions and direction to my thesis work.

I also would like to thank the following people, who are current or former members in the Microwave Photonics Research Group at the School of Information technology and Engineering: Dr. Jian Liu, Ms. Jian Yao, Mr. Zhichao Deng, and Mr. George Qi. Their excellent strong supports and generous help greatly improved my research work.

Special thanks also go to Optical Communications and Electro-photonics Group of the Communications Research Centre Canada and Bragg Photonics Inc for their numerous supports for fabrication of the FBG arrays.

Finally I am greatly indebted to my beloved family. They have always been the biggest support, physically and mentally, to my study.

LIST OF PUBLICATIONS

Refereed journal paper:

1. F. Zeng, J. P. Yao and S. Mihailov, "Genetic algorithm for fiber Bragg grating based all-optical microwave filter synthesis," SPIE Journal - Optical Engineering, vol. 42, no. 8, pp. 2250-2256, Aug. 2003.

Refereed conference papers:

2. F. Zeng, J. P. Yao and T. Yeap, "Dispersion effects and implementation errors on uniform fiber Bragg grating based true-time-delay beamforming networks," Proceedings of the International Topical Meeting on Microwave Photonics, pp. 337-340, Budapest, Hungary, Sept. 2003.

3. F. Zeng and J. P. Yao, "Dispersion effects of fiber Bragg gratings on true-time-delay beamforming networks," oral presentation at CCECE 2003, Montréal, Canada, May. 2003.

Chapter 1

INTRODUCTION

1.1 Background review

Signal processing for applications in the fields such as radar, communications can be projected to call for ever-increasing speed, bandwidth and dynamic range. Many applications also require small size, light weight and low power consumption. Analog signal processing [1] [2] continues to hold the promise to satisfy many of the requirements. Acoustic-wave delay line devices have been very widely used for signal processing applications. The most and sophisticated acoustic-wave delay line devices are those that use surface acoustic waves (SAW) [3] [4]. Planar processing techniques can be used to fabricate SAW transversal filters with thousands of taps and can operate at frequencies about several hundreds megahertz. Magneto-static-wave (MSW) devices [2], which make use of propagation of slow and dispersive spin waves in low-loss ferromagnetic materials, can operate at frequencies in the range of 2-12 GHz with bandwidth on the order of 1 GHz. Super-conducting delay-line (SDL) filters [5], using niobium transmission lines and proximity coupler taps, promise to offer low-loss devices with bandwidth about 20 GHz. Digital signal

processing is probably the most widely used approach nowadays for signal processing, however, its processing speed is normally less than several GHz [1] [6] [7]. This limitation stems from the fact that the required sampling speed increases in direct proportion to the bandwidth of the RF signal to be processed. Being important, the electronic bottleneck is by no means the only source of limitation, since electromagnetic interference (EMI) and frequency dependent losses can also be sources of important impairments. Compared with the approaches discussed above, all-optical signal processing is generally recognized to be needed in order to fully exploit the advantages provided by fiber-optic systems and networks, such as low loss, low dispersion, light weight, high time-bandwidth product, and immunity to EMI [8] [9]. In addition, the capability of processing high frequency and wideband signals directly in the optical domain, without the need for inefficient and costly intermediate conversions to and from the optical and electrical domains, can be of great practical value for potential applications including the direct interfacing of fiber processors with high-speed optical communication systems and radio over fiber networks.

For these reasons, there is considerable interest in optical fiber signal processors for a number of frequency- and time-domain applications, such as filtering [8-9] [17-18] [22-30] [32-46], correlation [12] [15-16], matched

filtering [13-14], and Fourier transformation [10] [11]. The original of fiber delay line signal processing can be traced back to the seminal paper of Wilner and Van den Heuvel [9] in 1976, who noted that the low loss and high modulation bandwidth of optical fibers is suitable for broadband signal processing. Intense research work on photonics microwave signal processing has been carried since 1980's, with the development of some key optical components, such as doped fiber amplifiers (DFA), high speed external modulators and fiber Bragg gratings (FBGs). Different delay line filter configurations have been proposed, in which the tapping elements can be optical couplers [23] [63-66], Mach-Zehnder lattices [21] [24] [67], high dispersion fibers [18] [20] [22] [51], Arrayed waveguide (AWG) [39] [52], or FBGs [25-27] [30-32] [34-35] [38] [40-43] [48-49]. Among these tapping elements, FBGs have been considered a good candidate for all-optical microwave filtering because of the numerous advantages provided by FBGs. In FBG-based delay line filters, the tapping intervals can be easily manipulated by controlling the grating spacing, and the tapping weights can also be controlled by varying grating reflectivity during the FBG fabrication process. In addition, the interaction wavelength can be controlled or tuned via changing the grating pitch by applying strain [55-58], which can be realized by variable heating, piezoelectric controlling, mechanical controlling or magnetic field controlling. Furthermore, by using wide-band chirped fiber Bragg gratings as

dispersion elements, more sophisticated tunability can be achieved. All these features make the synthesis of wideband FBG-based all-optical microwave filters with easy reconfigurability and tunability possible.

1.2 Objectives of this research

In an all-optical microwave filter, the microwave signals are carried by an optical carrier, usually incoherent. The optical carrier has a frequency thousands of times greater than that of the microwave signals. Photodetectors are square-law devices that respond to the incident optical power and none is fast enough to respond to the optical frequency and phase. All-optical microwave filters incoherently combine tapped optical signals. Although, in principle, coherent processing [19] [33] [62] can be used for all-optical signal processing, it is difficult to implement such a coherent system in practice. One important consequence of incoherent detection in all-optical microwave filters is that negative coefficients cannot be realized optically. For all-optical microwave filter design, since no negative filter coefficients can be used, standard digital filter design algorithms cannot be applied readily. The objectives of this research are to design FBG-based all-optical microwave filters using genetic algorithms, and to implement the filters. In order to make

the FBG-based all-optical filters operate at higher frequencies, the dispersion effects caused by the FBGs have to be considered.

1.3 Major contributions

1. The synthesis of FBG-based all-optical microwave filters using the genetic algorithms is proposed. In the proposed algorithms, all-optical microwave filters employing fiber Bragg gratings as tapping and weighting elements are considered. The coefficients and the tapping intervals of the microwave filters are optimized by the genetic algorithms. Algorithms for fixed and variable tapping intervals are developed and two design examples are presented and discussed.

2. Two FBG arrays are fabricated based on the design using the genetic algorithms. All-optical microwave filters based on the two FBG arrays are constructed and characterized. To achieve the optimal filter response, the filter coefficients have to be calibrated. We show that by considering the power spectrum of the optical source and the power reflectivities of the FBGs, the filter response identical to the design objective is achieved.

3. Dispersion effects on the performance of uniform FBG-based all-optical microwave filter are discussed. We show that the dispersion effects can be reduced or almost eliminated if single-side band modulation scheme is used. For double-side band modulation, the dispersion effects can be reduced by using short and weak fiber Bragg gratings.

1.4 Organization of this thesis

This thesis consists of six chapters. In Chapter 1, a brief review of the historical background of optical signal processing is first presented, followed by the objectives and major contributions of this research. In Chapter 2, the theory model of uniform FBG-based all-optical microwave filter is presented, showing the relationship between the system transform function and characteristics of the uniform FBGs. The key components such as electro-optic modulators, photodetectors, FBGs are introduced in this chapter. Genetic algorithms for FBG-based microwave filter synthesis are introduced in Chapter 3, two design examples are given. In Chapter 4, two FBG arrays are fabricated based on the two design examples. Experimental implementation of the all-optical microwave filters using the two FBG arrays is carried out. To achieve an optimal filter response, the filter coefficients have to be calibrated based on the power spectrum of the optical source and the power reflectivities

of the FBGs. Dispersion effects of the uniform FBGs on the performance of the all-optical microwave filters is discussed in Chapter 5. The dispersion effects can be reduced or almost eliminated if single-side band modulation scheme is used. For double-side band modulation, the dispersion effects can be reduced by using short and weak fiber Bragg gratings. Finally, a conclusion is drawn in Chapter 6 with recommendations for future work.

Chapter 2

THEORY MODEL

2.1 Basic concepts

The basic concepts of delay-line transversal filters will be introduced, followed by the magnitude characteristics of a typical low-pass filter. The fundamental structure of all-optical microwave filters will be addressed. Electro-optic modulator (EOM) and photodetector are the key components in all-optical microwave filters. Their mathematical models are introduced in Sections 2.1.3 and 2.1.4.

2.1.1 Delay-line transversal filters

Let us consider delay-line signal processors with the Direct Form I structure [6] [7], as shown in Fig 2.1. It is composed of two cascaded blocks, the first block is a Finite Impulse Response (FIR) filter and the second block is an Infinite Impulse Response (IIR) filter. The difference equation that relates the output signal $y(t)$ to the input signal $x(t)$ is given by

$$y(t) = \sum_{k=1}^{N} a_k y(t-kT) + \sum_{k=0}^{M} b_k x(t-kT), \tag{2.1}$$

where T is the unit time delay, a_k and b_k are tapping weights, or filter coefficients.

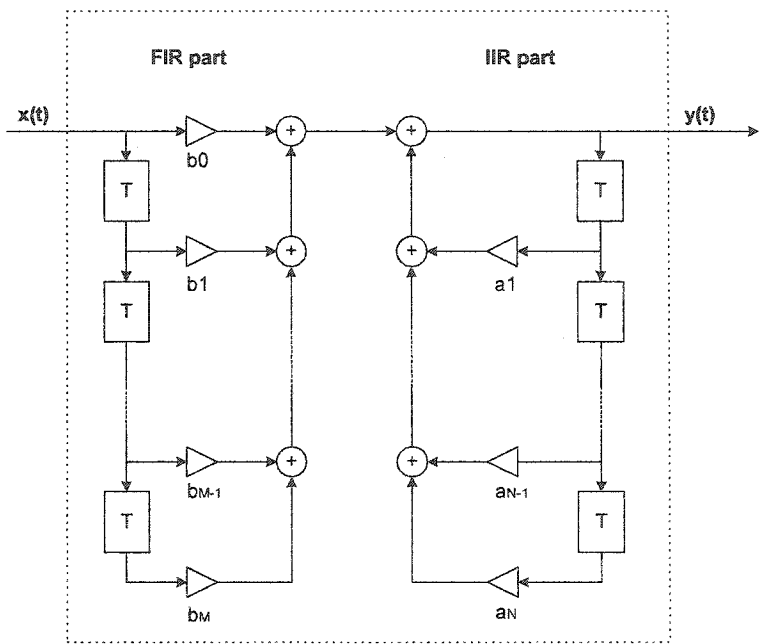

Fig 2.1 Block diagram representation for a Direct Form I filter.

The spectral characteristics of this structure can be analyzed using the well-known system function, which is obtained by applying the Fourier transform to both sides of Eq. (2.1)

$$H(\omega)=\frac{Y(\omega)}{X(\omega)}=\frac{\sum_{k=0}^{M} b_k e^{-j\omega kT}}{1-\sum_{k=1}^{N} a_k e^{-j\omega kT}}. \qquad (2.2)$$

The numerator represents the FIR part, whereas the denominator accounts for the IIR part. M and N stand for the order of the FIR and IIR respectively. The filter design problem is to approximate any of the ideal frequency response characteristics with a system that has the frequency response in Eq. (2.2), by properly selecting the coefficients $\{a_k\}$, $\{b_k\}$ and T. The free spectral range (FSR) defined as the inverse of unit time delay T. If $a_k = 0$ for all k, the filter is non-recursive and it is usually known as a transversal filter or a moving average (MA) filter, which consists only of feed-forward paths and has only zeros on Z-plane [6] [7]. In this thesis, transversal filter is chosen since it is a very generic filter architecture that may be adapted to realize various filtering functions. In addition, FIR filters can have a generalized linear phase, which is particularly desirable in many applications.

The magnitude response of a low-pass filter is illustrated in Fig 2.2. The band-edge $f_{pass}T$ defines the edge of the pass-band, while $f_{stop}T$ denotes the beginning of the stop-band. The transition of the frequency response from pass-band to stop-band defines the transition-band, which is calculated to be

$f_{stop}T - f_{pass}T$. The ripple in the pass-band of the filter is denoted as δ_1, and the magnitude $|H(\omega)|$ varies between the limits $A_{pass} \pm \delta_1$. The ripple in the stop-band is denoted as δ_2.

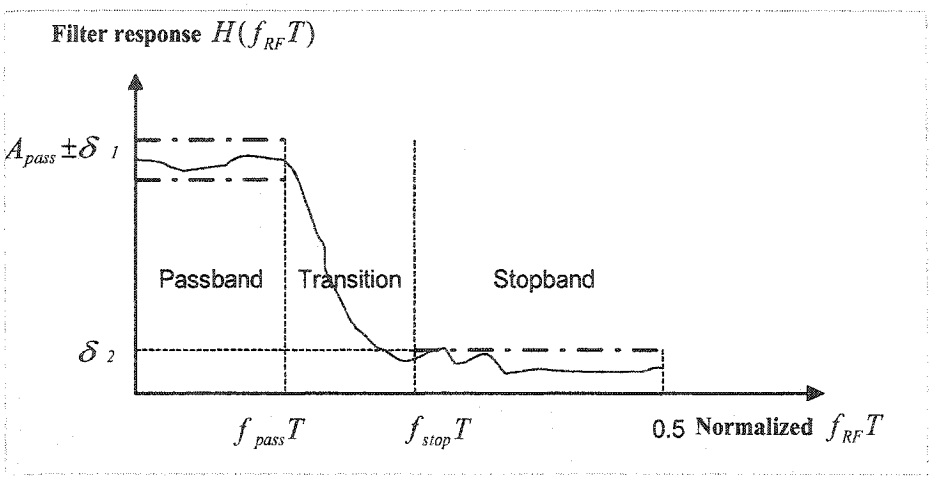

Fig 2.2 Frequency-domain low-pass filter design specifications.

The degree to which the transfer function $|H(\omega)|$ approximates the specifications depends in part on the criterion used in the selection of the filter coefficients $\{b_k\}$ as well as the number of coefficients used. The filters can be easily implemented using digital electronics. Numerous algorithms have been proposed and some of them are commercially available, such as the window method [6] [7] in time domain, and the least squares design method [6] [7] in frequency domain. For all-optical microwave filter, however, standard digital filter design algorithms cannot be applied readily because incoherent

interference prevents the inclusion of negative coefficients. In the next section, we will give the general architecture of all-optical delay line microwave filters and explain why the negative coefficients are not available in these filters.

2.1.2 All-optical microwave transversal filters

An all-optical delay line filter usually has the same structure as the FIR part of the Direct Form I filter shown in Fig 2.1. In general, an all-optical microwave transversal filter has an optical source, usually incoherent, a tapped delay-line device, and a photodetector, as shown in Fig 2.3. Input electrical signal $x(t)$ is modulated onto the incoherent light source via an external modulator. The modulated light is sent to the tapped delay line device. The variable optical attenuators can be used to change the tapping weights. The time delayed signals are then incoherently multiplexed in the second star coupler and detected at the photodetector. The optical power output of the delay-line filter is linearly proportional to the input optical power, provided that there are no nonlinear effects in the system. The entire system can be treated as a linear, time-invariant system in which the output is the convolution of the input electrical signal $x(t)$ with impulse response of the filter.

It is worthwhile to point out that we use "incoherent" light source and "incoherent" multiplexing to describe the all-optical microwave filters. A fundamental distinction must be made here on the all-optical microwave filter operation regime in terms of the relationship between the coherence time τ_c of the light source and the unit delay T, which is denoted as the time between adjacent taps. In general, the coherence length l_c of the source is given

$$l_c = \tau_c \cdot c \approx \lambda^2 / \Delta\lambda; \tag{2.3}$$

where c is the speed of light in free space, λ is the center wavelength, and $\Delta\lambda$ is the spectral bandwidth of the light source. If $\tau_c >> T$ or $l_c >> l$ (the spacing between any adjacent tapping elements), the filter is said to work under coherent regime and its transfer function partially depends on the optical phase shifts experienced by the carrier. Theoretically, in this situation, it is possible to obtain negative tapping weights by applying coherent detection. However, those optical carrier phase shifts are highly dependent on environmental parameters and polarization, which makes their implementation difficult under realistic conditions. On the contrary, if $\tau_c << T$ or $l_c << l$, the light source is said to be incoherent and the filter works under incoherent regime. In this situation, the effects of optical phase shifts can be discarded

and the filter transfer function is only linear in terms of the optical intensity. Then only non-negative coefficients can be achieved. In this thesis, we focus on incoherent fiber design and implementation, since it is more prone to practical implementation. Nevertheless, it is not necessary to have a completely coherent light to produce an interference pattern. Under certain conditions, an interference pattern may be produced from an incoherent source. For example, a degree of temporal coherence can be obtained by using a Mach-Zehnder interferometer structure, which is also understood as the principle of an incoherent light source being intensity modulated by an external electro-optic modulator. More details of this intensity modulation will be described in the following section.

As can be seen from Fig 2.3 the electro-optic modulator, the photodetector, the light source and the tapped delay-line device are the key components in the all-optical microwave filters. In the following we will first introduce briefly the principle of the electro-optic modulator and the photodetector. The light source can be light emission diode (LED), laser array, or amplified spontaneous emission (ASE) of an erbium doped fiber amplifier (EDFA). In this research project, ASE of an EDFA will be applied and fiber Bragg gratings (FBGs) will be used as the tapped elements, which will be described in Section 2.2.

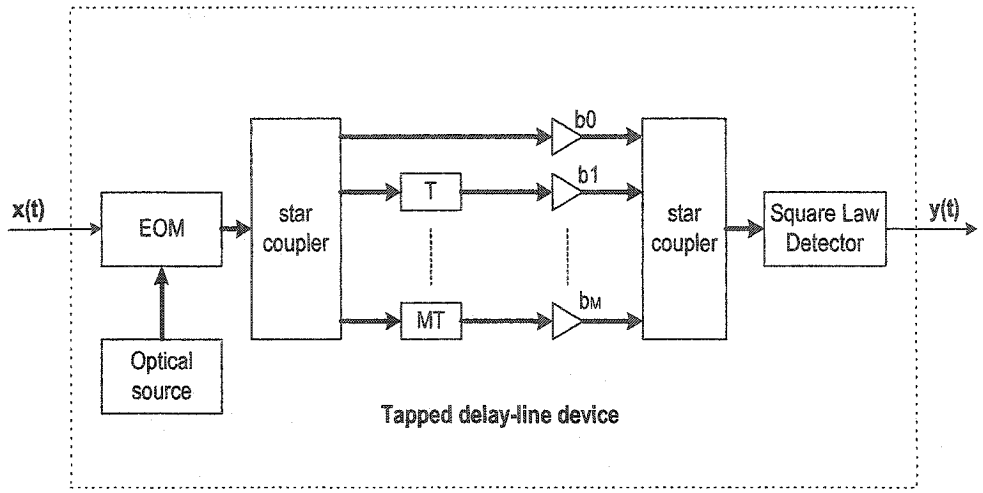

Fig 2.3 Generalized all-optical microwave filter that includes an optical source, tapped delay-line device, and photodetector.

2.1.3 Electro-optic Modulator

The principle of electro-optic modulators is based on the electro-optic effect, which induces a change in the refractive index proportional to an externally applied electrical field E [53] [54]. In our experiments, Lithium Niobate ($LiNbO_3$) intensity modulator is used. $LiNbO_3$ is known as Pockels medium or non-Centro-symmetric crystal. Its refractive index will change when an electric field E is applied to the crystal:

$$\delta_n(E) = -\frac{1}{2} r n^3 E, \tag{2.4}$$

where $\delta_n(E)$ is the variation of refractive index as the function of applied electrical field E, r is the electro-optic effect coefficient and n is the effective refractive index of this medium. An intensity modulator can be achieved by using a phase modulator in a Mach-Zehnder interferometer shown in Fig 2.4.

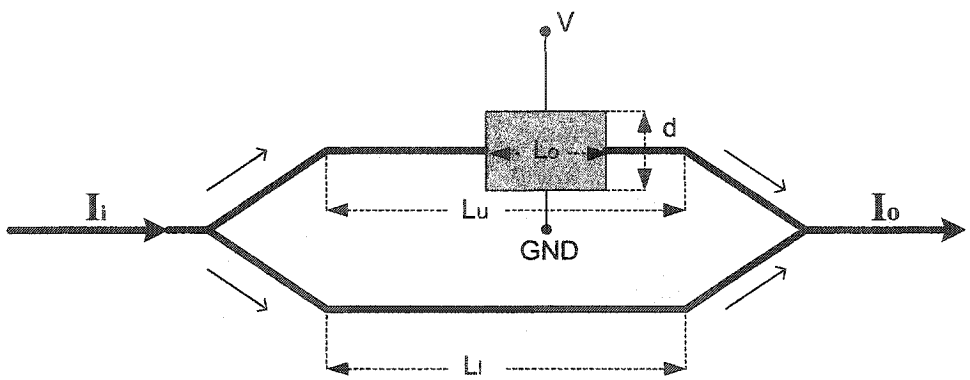

Fig 2.4 Block diagram of a Mach-Zehnder interferometer based electro-optic modulator.

The phase modulator is located at the upper branch, which introduces a phase shift Φ_u to the light propagated through the upper branch. Φ_u is expressed as

$$\Phi_u = \Phi_{uo} + \Phi_E = \frac{2\pi n L_u}{\lambda_0} - \frac{2\pi \delta_n(E) L_0}{\lambda_0}, \tag{2.5}$$

where L_u is the total length of the upper branch, and L_o is the length of the Pockels cell to which an electric field E is applied, λ_0 is the wavelength of the incident light, Φ_{uo} is the phase shift of the light after propagating through length L_u and Φ_E is the phase shift induced by the refractive index change within L_o. Using Eq. (2.4) we have

$$\Phi_u = \frac{2\pi n L_u}{\lambda_0} - \pi \frac{r n^3 E L_0}{\lambda_0}. \tag{2.6}$$

The phase shift Φ_l caused by the lower branch is

$$\Phi_l = \frac{2\pi n L_l}{\lambda_0}, \tag{2.7}$$

where L_l is the total length of the lower branch.

If the beam splitter splits the beam power equally, the transmitted intensity I_{mod} is related to the input intensity I_{in} by

$$I_{\text{mod}} = \frac{1}{2} I_{in} + \frac{1}{2} I_{in} \cos(\Phi) = I_{in} \cos^2(\frac{\Phi}{2}), \tag{2.8}$$

where $\Phi \equiv \Phi_u - \Phi_l = \frac{2\pi n(L_u - L_l)}{\lambda_0} - \pi \frac{rn^3 EL_0}{\lambda_0}$ is the phase difference between these two arms.

An important parameter named half-wave voltage V_π, a voltage at which Φ_E equals π, is defined as

$$V_\pi = \frac{d}{L_0} \cdot \frac{\lambda_0}{rn^3}, \tag{2.9}$$

where L_o is the length of the Pockels cell, d is the distance separating the two faces of the Pockels cell across which the electric field is applied. Using $E = V/d$, we obtain the transmittance of this modulator, $\mathrm{T}(V)$, defined as the ratio between the output optical intensity and input optical intensity,

$$\mathrm{T}(V) = \cos^2\left(\frac{\Phi_0}{2} - \frac{\pi}{2} \cdot \frac{V}{V_\pi}\right), \tag{2.10}$$

where $\Phi_0 \equiv \frac{2\pi n(L_u - L_l)}{\lambda_0}$, and V is the voltage of the modulating electrical signal. If $\Phi_o = \pi/2$, the modulator works in the nearly linear region around $\mathrm{T}(V) = 0.5$. Fig 2.5 shows the transmittance versus the applied voltage.

If the modulator is operating at the region around point B, the device acts as a linear intensity modulator. Then Eq. (2.8) can be approximated as

$$I_{\text{mod}} = \frac{I_{in}}{2}[1 + m_i \cdot x(t)], \tag{2.11}$$

where m_i is the intensity modulation index, and $x(t)$ is the electric signal shown in Fig 2.5.

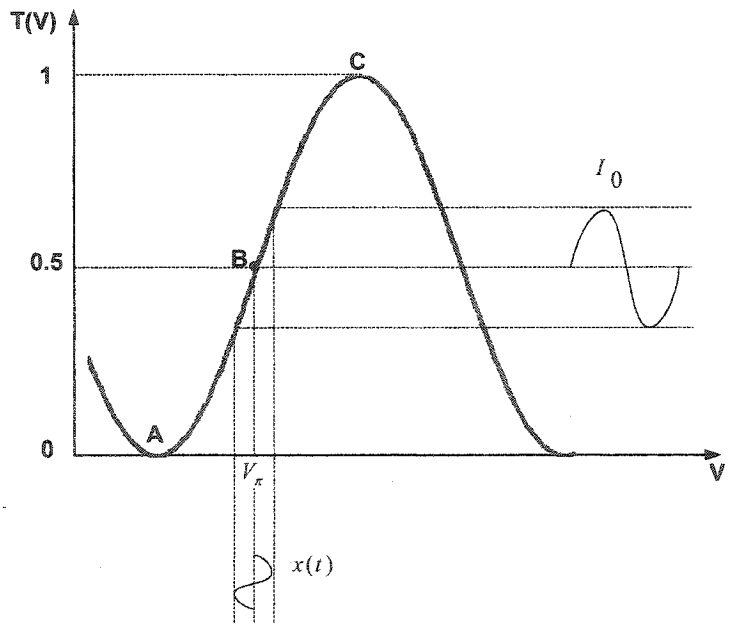

Fig 2.5 Transmittance of intensity modulator vs. the applied voltage.

We know that the optical intensity is proportional to the square of the amplitude of the optical electrical field. And if we further normalize $x(t)$ as $\cos(\omega_m t)$, the output optical electrical field of the modulator E_{mod} can be expressed as

$$E_{\text{mod}} = \sqrt{1 + m_i \cos(\omega_m t)} \cdot E_{in} \cdot e^{j(\omega_0 t + \varphi_0)}, \tag{2.12}$$

where ω_m is the modulating angular frequency of the RF signal, ω_o is the optical carrier angular frequency, φ_o is the initial phase of the carrier, and E_{in} is the amplitude of the input optical electrical field. Comparing with the m_i in Eq. (2.11), m_i in Eq. (2.12) is the normalized intensity modulation index which already accounts for the amplitude of the RF signal.

In view of the preceding derivation, Eq. (2.11) and Eq. (2.12) are obtained for a monochromatic source with wavelength λ_0. If a broadband light source consisting of many carrier frequency components incidents into this external modulator, and we further assume that each frequency components are incoherent with each other, the output optical electrical field can be considered as the sum of all the components. Since each component is different from λ_0 by a very small fraction of λ_0, the corresponding normalized intensity

modulation index for each carrier component is a little bit different with m_i. But without loss of generality, Eq. (2.11) is holding and it will be modified and used in Section 2.2 to derive the system transfer function of all-optical microwave filters, where m_i is assumed to be a constant to all carrier components. Similarly, in order to analyze the dispersion effects of the fiber Bragg gratings on the performance of all-optical microwave filters, Eq. (2.12) will be deformed to represent the optical electrical field of modulated broadband light in Chapter 5.

2.1.4 Photodetector

Fig 2.6 shows the basic structure of a PIN photodetector [53] [54]. The photodetector consists of an intrinsic semiconductor layer sandwiched between p-doped and n-doped layers. The photodetector is reversibly biased to increase the thickness of the depleted region, which results in a large internal electric field. When light is incident on the photodetector, and if the photon energy is greater than the band gap of the semiconductor material, it can be absorbed and generate a pair of electron-hole, photo current is generated.

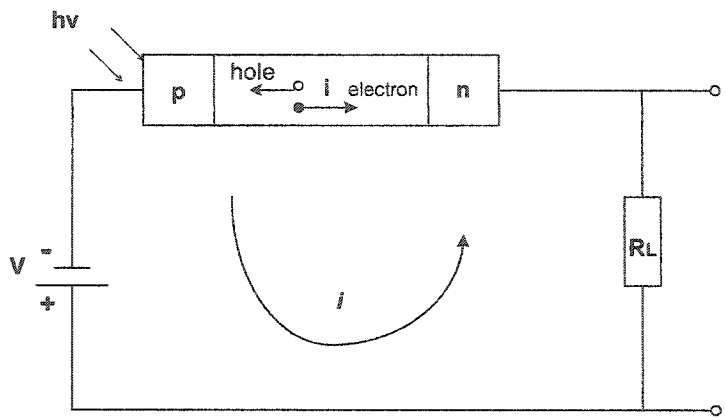

Fig 2.6 Structure of the PIN photodetector.

The photo-generated current i_p and input optical power P_i have the relations

$$i_p = \frac{\eta \cdot q}{h\nu} \cdot P_i = \Re \cdot P_i, \tag{2.13}$$

where η is the quantum efficiency, h is the plank constant, ν is the frequency of carrier photon, and q is the charge of an electron. $\Re \equiv \frac{\eta q}{h\nu}$ is defined as the responsivity of the photodetector.

For example, when an optical signal described by Eq. (2.12) is incident on this photodetector, the output electric signal, either voltage or current, may be expressed as

$$y(t) = \frac{\int_{\Delta t} |E_0(t)|^2 dt}{\Delta t} \cdot \Re = A_0 + A \cdot \cos(\omega_m t), \tag{2.14}$$

where Δt is the response time of the photodetector with $2\pi / \omega_m >> \Delta t >> 2\pi / \omega_0$; A_0 is defined as the dc component and A is the amplitude of the recovered RF signal.

Ideally, the photodetector can exactly recover the modulated RF signal if shot noise and thermal noise are neglected, and no dispersion and chirp effects during the modulation and propagation process before the light is detected by the photodetector with infinite short response time. Otherwise, amplitude and phase distortions will be presented at the recovered signal. These effects will be discussed in Chapter 4 and Chapter 5.

2.2 Fiber Bragg grating based all-optical microwave filters

The tapped delay line is one of the key devices in an all-optical microwave filter and can be realized using optical couples, Mach-Zehnder Lattices, high dispersion fibers, uniform FBG arrays, or chirped gratings. In general, tapped delay lines can be divided into three groups. In the first group, a narrow band light source is used. The tapping components are a numbers of cascaded 2×2

directional couplers [62-69]. Because the coupling ratio of the 2×2 directional coupler is always less than one; in real systems, many of them are less than 0.5 or even smaller, the reduction of light after some stages is very significant, which may make it impossible to cascade more couplers to generate enough taps if no optical amplifiers are used. In addition, compulsory connection should be made between these couplers; therefore many connectors are needed which lead to high power loss and poor system reliability. Furthermore, the fiber length between adjacent couplers should be accurate in order to achieve accurate time delays, which makes the implementation difficult. In the second group, a multi-wavelength light source is used. The time delays are achieved using a high dispersion medium, such as a section of high dispersion fiber or a chirped grating. The light source is more difficult to obtain than that in the first group, but the tapped delay-line devices could have simpler structures. More important, the microwave filter based on the delay lines in this group can be easily tuned by changing the dispersion of the dispersion medium [99]. In the third group, a broadband light source is used. The tapped delay line can be realized in the third group using an array of FBGs. The use of FBGs for all-optical microwave filtering has numerous advantages. In FBG-based delay-line filters, the tapping intervals can be easily manipulated by controlling the grating spacing, and the tapping weights can also be controlled by varying grating reflectivity during the FBG fabrication process. In addition, the

interaction wavelength can be controlled or tuned via changing the grating pitch by applying strain. Considering the advantages offered by FBG-based microwave filters, in this thesis our attention is focused on the all-optical microwave filters based on the optical delay lines using an FBG array.

2.2.1 Fiber Bragg gratings

An FBG is a periodic perturbation of the refractive index along the fiber length. FBGs are fabricated by using either phase mask technique or holographic technique, by exposure of the fiber core to an intense ultraviolet (UV) optical interference pattern, to change the refractive index of the fiber core periodically. The refractive index profile of a uniform FBG is shown in Fig 2.7.

The refractive index variation profile of a uniform FBG $\delta_{neff}(z)$ can be written as [59]

$$\delta_{neff}(z) = \bar{\delta}_{neff}(z)\{1 + \nu\cos[\frac{2\pi}{\Lambda}z + \phi(z)]\}, \tag{2.15}$$

where $\overline{\delta}_{neff}(z)$ is the dc index change along grating length z, Λ is the period of the grating, ν is the modulation index, and $\phi(z)$ is the phase which is a constant in ideal condition. However, $\phi(z)$ may change along the length of the FBG, which leads to the chirping of the grating due to the fabrication errors. In many cases, only the fiber core is photosensitive, so the index change is assumed to be within the fiber core only.

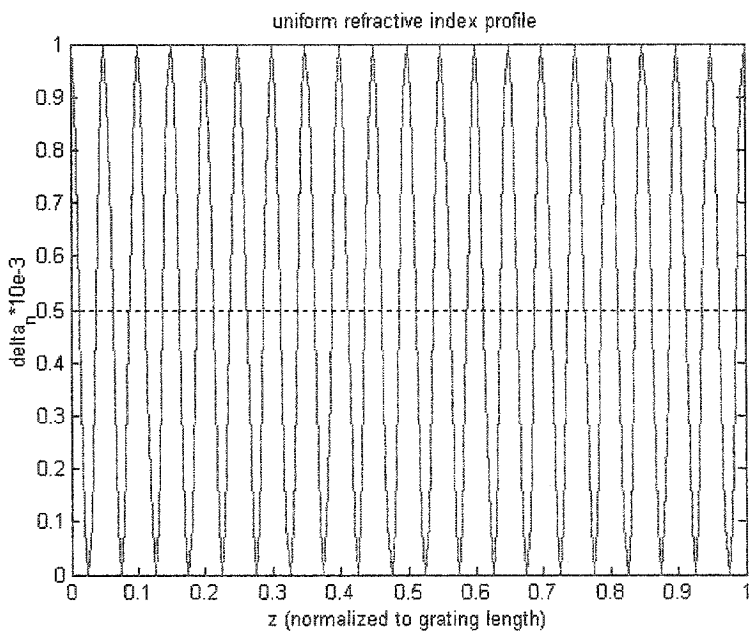

Fig 2.7 Refractive index profile of a uniform FBG with $\overline{\delta}_{neff} = 0.5 \times 10^{-3}$.

Fiber gratings can be broadly classified into two types: Bragg gratings and transmission gratings (long period gratings). In Bragg gratings, power

coupling occurs between modes traveling in opposite directions within the fiber core. In transmission gratings, the coupling occurs between modes traveling in the same direction in both the core and the cladding. In this research, Bragg gratings are used as tapping and weighting elements for the microwave filter design.

Basically, the coherent interference of partial reflectance within an FBG creates a band-pass reflection response and stop-band transmission response as shown in Fig. 8. The center wavelength of the reflection is called Bragg wavelength, which is related to the grating period by

$$\Lambda = \lambda_B / 2n_{eff}, \tag{2.16}$$

where λ_B is the Bragg wavelength and n_{eff} is the effective refractive index.

Because FBGs are the tapping and weighting components in the delay line filters, its characteristics will affect the performance of the FBG-based delay line filters. Coupled-mode theory [59-61] is a powerful tool to analyze the spectrum and phase of the FBGs. Through the analysis, many physical insights can be gained, and better understanding of the FBG characteristics would be achieved.

In an FBG fabricated in single-mode fiber; near the Bragg wavelength for which reflection of a mode of amplitude $A(z)$ into an identical counter-propagating mode of amplitude $B(z)$ is the dominant interaction. The coupled-mode equations are developed to describe the change in amplitude of the forward and reverse waves [59]:

$$\begin{aligned} \frac{dR}{dz} &= j\hat{\sigma}R(z) + j\kappa S(z) \\ \frac{dS}{dz} &= -j\hat{\sigma}S(z) - j\kappa^* R(z) \end{aligned}, \tag{2.17}$$

where $R(z) \equiv A(z)\exp(j\delta z - \phi/2)$ and $S(z) \equiv B(z)\exp(-j\delta z + \phi/2)$, κ is the "ac" coupling coefficient and $\hat{\sigma}$ is the general "dc" self-coupling coefficient given by

$$\hat{\sigma} \equiv \delta + \sigma - \frac{1}{2}\frac{d\phi}{dz}. \tag{2.18}$$

The detuning δ, which is independent of z, is defined as

$$\delta \equiv \beta - \frac{\pi}{\Lambda} = 2\pi n_{eff}\left(\frac{1}{\lambda} - \frac{1}{\lambda_B}\right), \tag{2.19}$$

where β is the propagation constant.

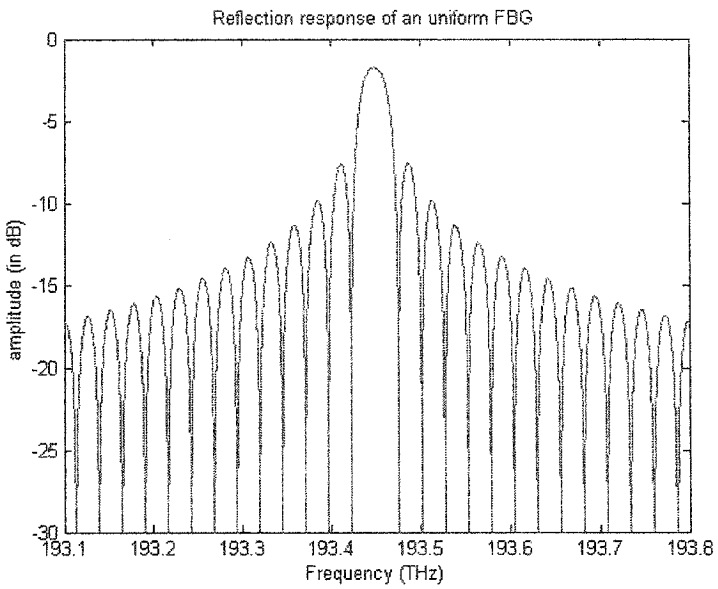

(a)

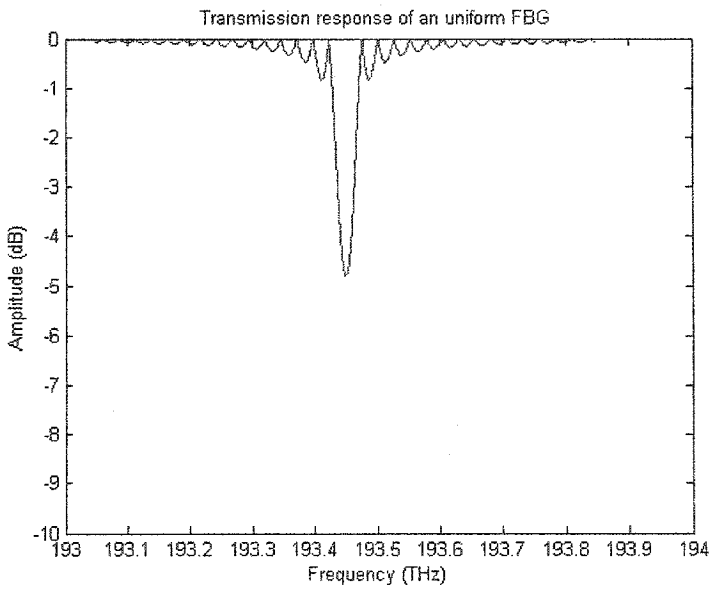

(b)

Fig 2.8 Simulated FBG response of a uniform FBG with 4-mm long and $\overline{\delta}_{neff} = 1 \times 10^{-4}$ (a) Reflection response (b) Transmission response.

We also have the following simple relations,

$$\begin{aligned} \sigma &= \frac{2\pi}{\lambda}\bar{\delta}_{neff} \\ \kappa &= \kappa^* = \frac{\pi}{\lambda} v \cdot \bar{\delta}_{neff} \end{aligned}, \tag{2.20}$$

where κ^* is denoted as the conjugate of "ac" coupling coefficient κ. It can be seen from Eq. (2.18) and Eq. (2.19), the "dc" self-coupling coefficient $\hat{\sigma}$ depends on the Bragg wavelength λ_B, the average index change $\bar{\delta}_{neff}$, and the grating chirp $d\phi/dz$. For a uniform grating, ϕ and $\bar{\delta}_{neff}$ are constant, and the coupled-mode equations have an analytic solution. The amplitude reflectance ρ for a uniform Bragg grating of length L is given by

$$\rho = \left.\frac{S(0)}{R(0)}\right|_{S(L)=0} = \frac{-j\kappa \sinh(\gamma L)}{\gamma \cosh(\gamma L) + j\hat{\sigma} \sinh(\gamma L)}, \tag{2.21}$$

where $\gamma \equiv \sqrt{\kappa^2 - \hat{\sigma}^2}$. The maximum reflection, defined as the peak reflectivity, occurs at $\hat{\sigma} = 0$, corresponding to a wavelength of $\lambda_{\max} = (1 + \delta_{neff}/n_{eff})\lambda_B$. The peak reflectivity R is given by

$$R = |\rho|^2 = \tanh^2(\kappa L). \tag{2.22}$$

The reflection bandwidth $\Delta\lambda$ is defined as the distance between the first two zeros of the reflection spectrum and is given by

$$\frac{\Delta\lambda}{\lambda_B} = \frac{v\bar{\delta}_{neff}}{n_{eff}} \sqrt{1 + (\frac{\lambda_B}{L v\bar{\delta}_{neff}})^2}, \tag{2.23}$$

where λ_B is the Bragg wavelength. And the power reflectivity is defined as the total reflected power within the null-to-null reflection bandwidth.

Bragg gratings are classified in terms of reflectance as weak or strong gratings. The weak grating regime is described by $v\bar{\delta}_{neff} << \lambda_B / L$. Its reflection bandwidth is given by $\Delta\lambda / \lambda \approx 2/\mathrm{N}$, where N is the number of periods, which means the bandwidth is inversely proportional to the grating length for weak gratings. In the strong grating regime, where $v\bar{\delta}_{neff} >> \lambda_B / L$, the reflection bandwidth is proportional to the index variation given by the ac index change, $\Delta\lambda / \lambda_B \approx v\bar{\delta}_{neff} / n_{eff}$, which means that the bandwidth for strong gratings is independent of grating length. These characteristics must be

considered during the design of all-optical microwave filters and the fabrication of FBG arrays, in order to achieve desired frequency response.

Furthermore, the phase and group delay characteristics, the first order or even higher order dispersion characteristics should also be considered. The dispersion effects on the performance of all-optical microwave filters will be discussed in Chapter 5.

2.2.2 System transfer function of FBG-based all-optical microwave filter

The function of the all-optical microwave transversal filter can be simply interpreted by using the grating array structure shown in Fig 2.9. The structure considered here consists of an optical circulator and an array of FBGs. Compared with the generalized structure shown in Fig. 2.3, the broadband source and the external electro-optic modulator are omitted in this diagram. The input of the FBG array is marked as "modulated broadband light" with the schematic diagram of its power spectrum. The FBG array is composed of a number of FBGs interconnected as the tapping elements of the transversal filter. Each FBG reflects a slice of modulated light at a specific wavelength from $\{\lambda_0, \lambda_1, \cdots, \lambda_M\}$, and the reflected time delayed signals are summed and

sent to photodetector. Also, the photodetector is omitted and the power spectrum of the reflected time delayed optical signals is sketched in Fig. 2.9. The electro-optic modulator, the photodetector and the FBGs have been discussed in Chapter 2. As mentioned in Chapter 2, the light source is also an important device for all-optical microwave filtering. In the following we will give a brief introduction to the light source used for the microwave filters.

First of all, let us consider that the light source is an ideal broadband light source with a flat power spectrum over the working wavelength range, that is

$$p_0(\lambda_0) = p_1(\lambda_1) = p_2(\lambda_2) = \cdots = p_M(\lambda_M) = p\,, \tag{2.24}$$

where $p_k(\lambda_k)$, $k = 0,1,2,\cdots,M$; is the optical power spectrum density at wavelength λ_k. The optical power over the working wavelength range launched from the light source is

$$\mathrm{P}_{BS} = \int_{\lambda_0}^{\lambda_M} p(\lambda)d\lambda = p\cdot(\lambda_M - \lambda_0)\,. \tag{2.25}$$

To simplify the analysis, we assume that the intensity modulation index m_i does not change for different wavelength within λ_0 and λ_M, and the electro-

optic modulator is operating at the linear region around the half-wave voltage. This assumption is a good approximation when the linear working region of this modulator is wide enough. Based on Eq. (2.11) and Eq. (2.25), the output optical power of the electro-optic modulator P_{EOM} is

$$P_{EOM} = \frac{1}{2} P_{BS}[1 + m_i x(t)] = \frac{1}{2} p \cdot (\lambda_M - \lambda_0) \cdot [1 + m_i x(t)], \tag{2.26}$$

where $x(t)$ is the electrical signal applied to the modulator.

The following assumptions can also be made for the analysis of the FBG-based microwave filters:

First, the spacing between any adjacent FBGs is identical, and the time delay between two adjacent FBG T is calculated by

$$T = \frac{2n_{eff} l}{c}, \tag{2.27}$$

where n_{eff} is the effective refractive index of the single mode fiber, l is the spacing between any adjacent FBGs, and c is the speed of light in free space.

Second, the power reflectivities $\{R_0, R_1, R_2, \cdots, R_M\}$ of the FBGs are within [0, 1] with identical and very narrow bandwidth $\Delta\lambda$, that is

$$\Delta\lambda_0 = \Delta\lambda_1 = \Delta\lambda_2 = \cdots \Delta\lambda_M = \Delta\lambda . \tag{2.28}$$

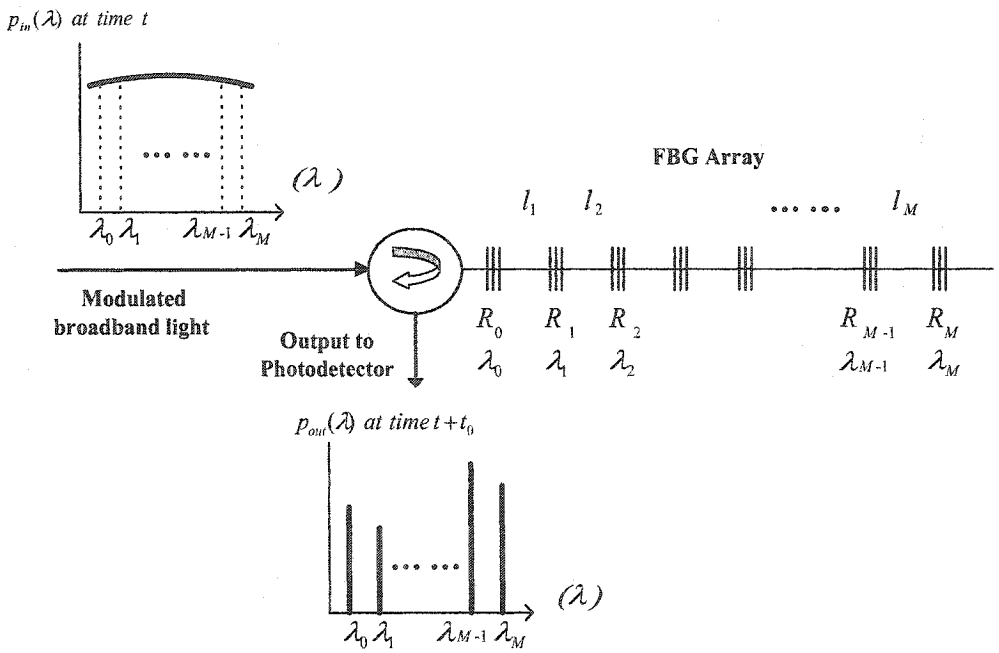

Fig 2.9 Basic structure of an FBG-based all-optical microwave filter.

Finally, the dispersion effects induced by the FBGs are not considered. We should note that when the frequency of the RF signal is very high, for example, greater than 10 GHz, the dispersion effects cannot be neglected. A detailed discussion on the dispersion effects will be presented in Chapter 5.

Based on the assumptions, the optical power of the modulated light after reflection by the FBG array is

$$\mathrm{P}_{RFL} = \sum_{k=0}^{M} \frac{p}{2} \cdot \Delta\lambda \cdot R_k + \frac{m_i}{2} \cdot p \cdot \Delta\lambda \cdot \sum_{k=0}^{M} R_k x(t - kT), \tag{2.29}$$

where R_k is the peak reflectivity at the k-th tap. The power spectrum density of reflected light is shown in Fig 2.9.

The electrical signal at the output of the photodetector is

$$y(t) = \Re \cdot \frac{1}{2} m_i p \Delta\lambda \cdot \sum_{k=0}^{M} R_k x(t - KT), \tag{2.30}$$

where $\Re$ is the responsivity of the photodetector.

Since we are only interested in the ac component, the dc component at the photodetector output is not included in Eq. (2.30). Applying Fourier transform on both sides of Eq. (2.30), we get the system transfer function

$$H_{desire}(\omega) = K \cdot \sum_{k=0}^{M} R_k e^{-j\omega kT}, \tag{2.31}$$

where $K \equiv \frac{1}{2}\Re mp\Delta\lambda$. Since K is only a scaling factor that does not affect the shape of the filter response, it can be ignored. $\{R_k\}$ with $k = 0, 1, 2, \cdots, M$ are the coefficients we are looking for. From Eq. (2.31) we can see that the transfer function of the filter is determined by the reflectivities of the FBGs. If the FBGs with the required reflectivities can be fabricated, all-optical microwave filters with the required transfer function or filter impulse response can be realized.

2.3 Summary

The basic concepts of delay-line transversal filters have been introduced. The fundamental structure of all-optical microwave filters was presented. The key components, such as the electro-optic modulator, the photodetector, the FBGs, and the light source, were introduced. The transfer function of the microwave filter using an array of FBGs was derived. It was found that the transfer function was completely determined by the peak reflectivities of the FBGs. This is the basis that we will use to synthesis and implement the all-optical microwave filters.

Chapter 3

FILTER DESIGN

As discussed in Section 2.1.1, any filter design problem can be considered as a task to find the coefficients $\{b_k\}$ and $\{a_k\}$, to best approximate the desired frequency response specifications, which includes 1) the maximum tolerable pass-band ripple, 2) the maximum tolerable stop-band ripple, 3) the pass-band frequency ω_{pass} and 4) the stop-band edge frequency ω_{stop}. The objective of this Chapter is to design an all-optical microwave transversal filter based on an array of FBGs by using genetic algorithms to satisfy the given specifications.

According to Fig 2.2, the transfer function of the microwave filter may be defined as

$$\left|H_{ideal}(\omega)\right| = \begin{cases} A_{pass}, & 0 \le fT \le f_{pass}T \\ Not\ concern, & f_{pass}T < fT < f_{stop}T \\ A_{stop}, & f_{stop}T < fT < 0.5, \end{cases} \tag{3.1}$$

where A_{pass} is between 1 ± 0.2 and A_{stop} should be less than 0.1; $f_{pass}T = 0.15$ and $f_{stop}T = 0.35$.

Digital filter design algorithms have been under intense investigation for years. Unfortunately, standard digital filter design algorithms cannot be applied readily to all-optical microwave filter synthesis because incoherent interference prevents the inclusion of negative coefficients in the all-optical microwave filter design. Several approaches have been proposed to solve this problem [63-69]. In Ref. 63, a state-space matrix representation of the problem was used in to enable the realization of general optical delay line topological structures. Capmany et al. [66] proposed to use the modified Padé approximation procedure to satisfy the desired response in time domain. In Ref. 67, a simpler technique was proposed to use a passive chain of non-uniform sections to produce a symmetrical window response in time domain. But none of these design methodologies attempt to produce filter structures which are optimal in terms of their physical size, or filter topology with variable tapping intervals, or the number of optical components used. To avoid these limitations, Cusick et al. [68] proposed using the genetic algorithms for microwave filter synthesis, but the designs [63-69] were carried out based on a number of 2 × 2 directional couplers. For 2 × 2 directional couplers, the coupling ratio is always less than one; in real systems, many of them are less

than 0.5 or even smaller. Because the reduction of light after some stages is very significant, it is not possible to cascade more couplers to generate enough taps. This feature limits the performance of all-optical microwave filters. In addition, the compulsory connection between these couplers requires the use of many connectors which lead to high power loss and poor system reliability. Furthermore, the fiber length between adjacent couplers should be accurate in order to achieve accurate time delays, which makes the implementation difficult. The use of FBGs for all-optical microwave filtering has numerous advantages. In FBG-based delay-line filters, the tapping intervals can be easily manipulated by controlling the grating spacing, and the tapping weights can also be controlled by varying grating reflectivity during the FBG fabrication process. In addition, the interaction wavelength can be controlled or tuned via changing the grating pitch by applying strain. Considering the advantages provided by FBGs, in this Chapter we propose to synthesize FBG-based all-optical microwave filters using genetic algorithms.

3. 1 Genetic algorithms

As numerical techniques from nature evolution, the genetic algorithms are well suited for simultaneous optimization of multivariable problems, which have the potential of obtaining near global optimum solutions [70-79]. Here

the genetic algorithms are pursuing to find out the optimal solution of $\{R_k\}$ to achieve an optimal approximation of $H_{desire}(\omega)$. Fig. 10 shows the diagram of the GA cycle. In the following, we describe the techniques that are employed in the GA process for encoding, fitness evaluation, parent selection and other genetic operations.

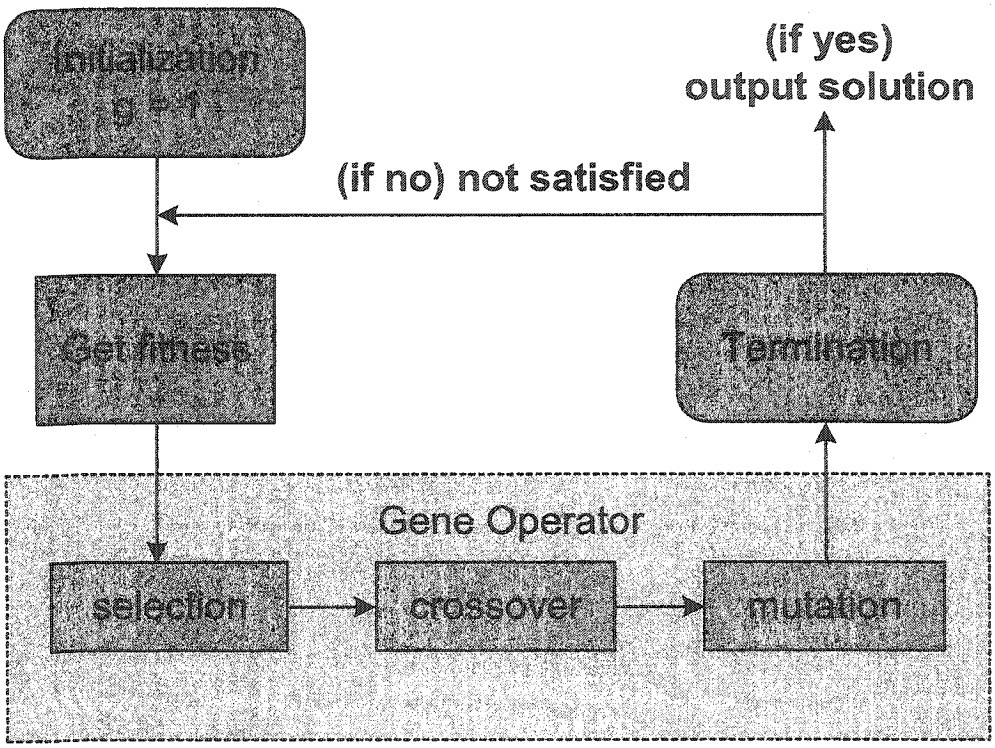

Fig 3.1 Diagram of a GA cycle.

First, generate an initial (g = 1) population of random binary strings of length $\sum_{k=0}^{M} L_k$, the first generation which is shown in Fig. 11, where $M+1$ is the

number of FBGs with unknown reflectivities, and L_k is the length of binary string required to represent the k 'th unknown variable. Each string is called a chromosome. Each chromosome is a trial solution of a list of the respective reflectivities of the FBGs in the delay line $\{R_0, R_1, R_2, ..., R_M\}$. And each bit of one chromosome is called a gene. The number of chromosomes in each population, called population size, is usually set as the bit length of each chromosome.

The method we use to provide a binary representation of the reflectivity is by a linear mapping between the real numbers and a binary representation of fixed length. That is

$$R_k = \frac{R_{\max} - R_{\min}}{2^{L_k} - 1} \cdot z_k + R_{\min}, \tag{3.2}$$

where $R_{\max}$ and $R_{\min}$ are maximum and minimum achievable FBG reflectivities, which can be set as the value which is available in practice. In ideal condition, $R_{\max} = 1$ and $R_{\min} = 0$. z_k is the decimal value representing the k-th section of the chromosome. This bit-string encoding method is the most classic approach used by GA thanks to its simplicity and traceability.

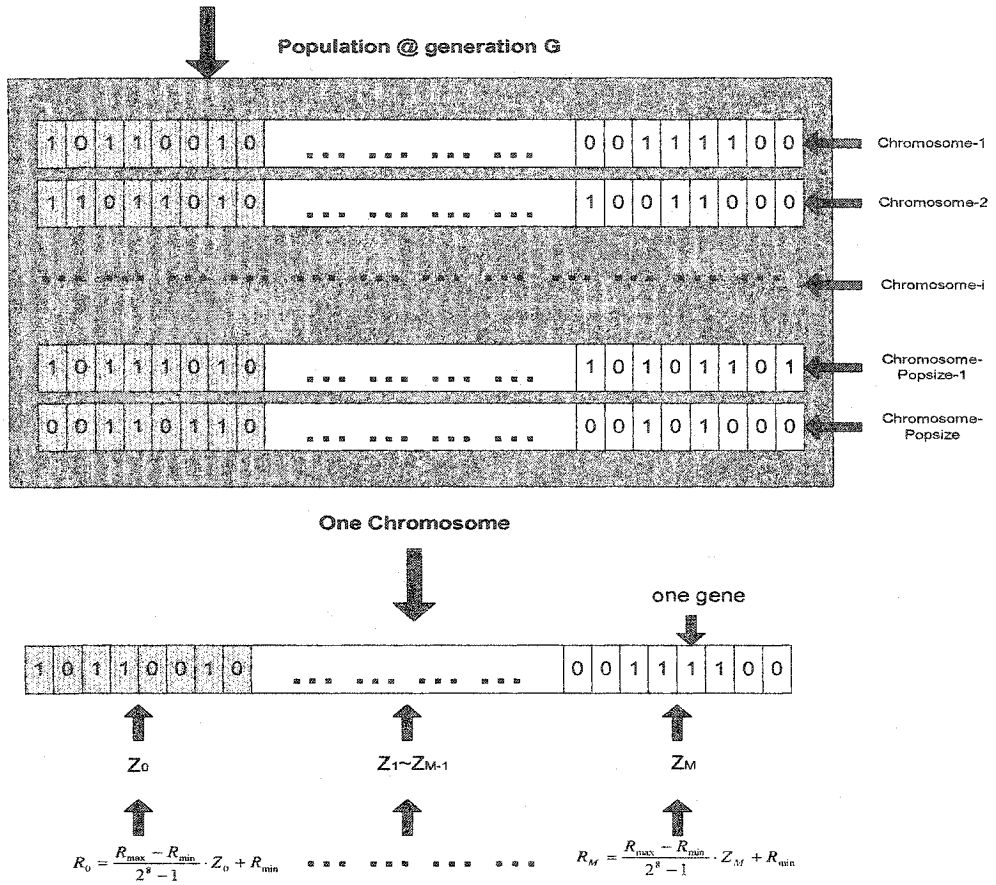

Fig 3.2 Diagram of population, chromosome and gene.

Next, decode each individual and test each of them in turn on the problem and convert the performance as fitness, where a better solution implies a higher fitness. Usually, two criteria are used to estimate the system transfer function.

1) The first one is the Minimum Maximum error (MM), which searches for the maximum peak error throughout a discrete frequency domain

by subtracting the magnitude response of the ideal filter from that of the designed filter, that is

$$error_{MM} = \max\{\|H_{ideal}(\omega)| - |H_{design}(\omega, \{R_k\})\|\}. \quad (3.3)$$

2) The second one is the Least Mean Square (LMS) error, which calculates the sum of the errors throughout the frequency domain by subtracting the magnitude response of the ideal filter from that of the designed filter.

$$error_{LMS} = \{\sum_{\omega}[|H_{desire}(\omega)| - |H_{design}(\omega)|]^2\}^{1/2}. \quad (3.4)$$

Fitness is defined as

$$fitness = \frac{1}{error}. \quad (3.5)$$

In order to reduce the error at frequencies that are most important such as the pass-band and stop-band and relax the error in "don't care" region such as the transition-band, a weighting function $W_{err}(\omega)$ may be introduced. Then Eq. (3.3) and Eq. (3.4) can be re-written as

$$error_{MM} = \max\{W_{err}(\omega)\cdot\left\|H_{ideal}(\omega)\right| - \left|H_{design}(\omega,\{r_n\})\right\|\}, \tag{3.6}$$

and

$$error_{LMS} = \{\sum_{\omega} W_{err}(\omega)[\left|H_{desire}(\omega)\right| - \left|H_{design}(\omega)\right|]^2\}^{1/2}. \tag{3.7}$$

For example, if we want to suppress more ripples in stop-band, the weight function may be selected as

$$W_{err}(\omega) = \begin{cases} 1, & pass-band \\ 0, & transition-band \\ \beta, & stopband \end{cases}, \tag{3.8}$$

where β should be greater than one. The corresponding simulation results are shown in Fig 3.3. It can be seen that increasing the weight of stop-band from $\beta = 1$, $\beta = 5$ to $\beta = 10$, the magnitude responses of the filter in stop-band decrease accordingly, but this also leads to the degeneration of the filter response in the pass-band. Therefore, for the given filter specifications, the weight function $W_{err}(\omega)$ should be carefully chosen to satisfy all requirements over the whole frequency range.

The MM error criterion and the LMS error criterion are compared during the filter design. Although using both criteria can finally achieve the design objective, we find that MM strategy generates better results than LMS, because MM criterion results in the maximum error spreading uniformly over the interval, giving an equal-ripple design, which is shown Fig 3.4.

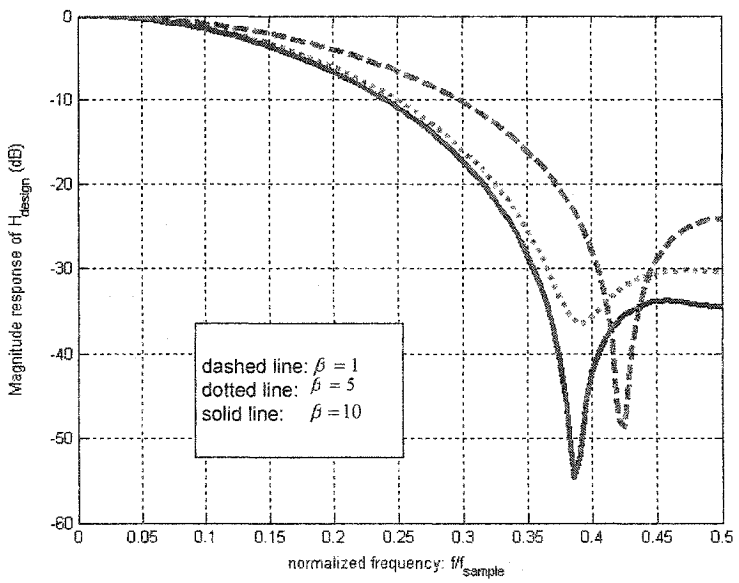

Fig 3.3 Design examples using MM error criteria with different weight function.

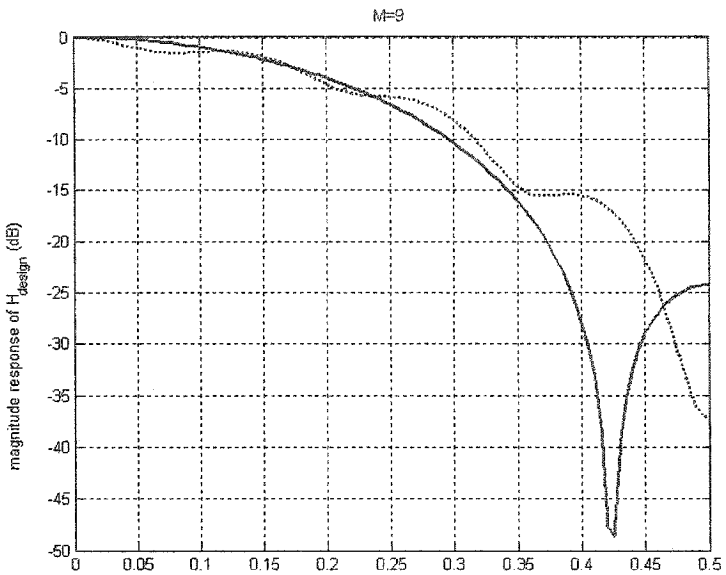

(a) $\beta = 1$

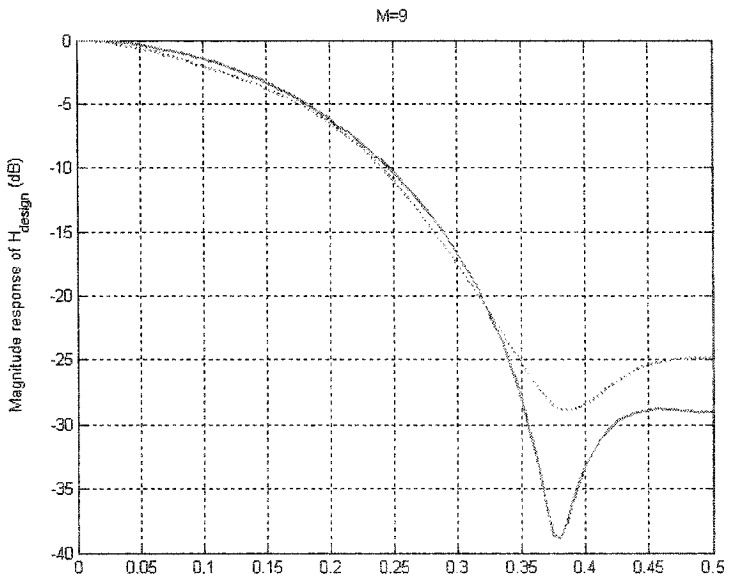

(b) $\beta = 5$

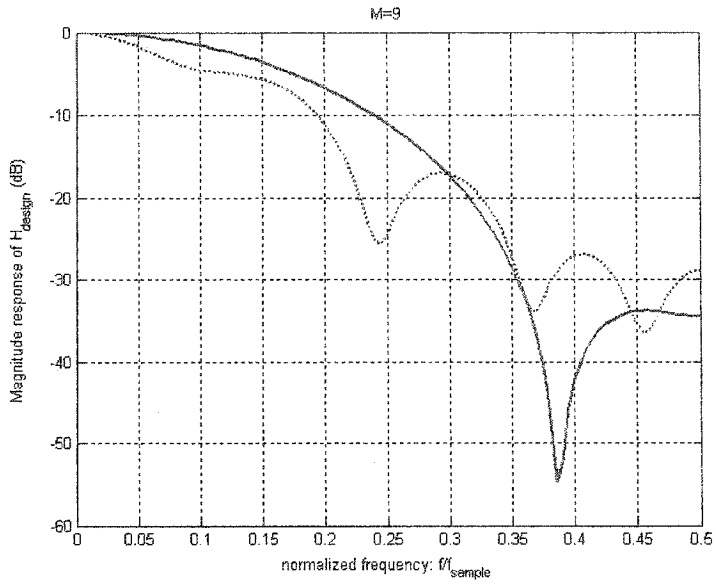

(c) $\beta = 10$

Fig 3.4 Design examples using the MM and LMS error criteria with different stop-band weights. (M=9; Dotted line: LMS; Solid line: MM.)

Third, the evolution operation (or Gene operator)

1) *Selection:* copies of individual solutions are made in numbers proportional to their relative fitness, which means chromosomes with better performance will have higher probability to be selected to reproduce.

2) *Crossover:* randomly choose pairs of individuals and apply with probability P_c single point crossover. Repeat until a new temporary

population of popsize chromosomes is formed. This operation is illustrated in Fig 3.5.

3) *Mutation* (shown in Fig 3.6): Random changes are made to a proportion of the bits in the population, to simulate mutation. The probability of mutation is defined as P_m.

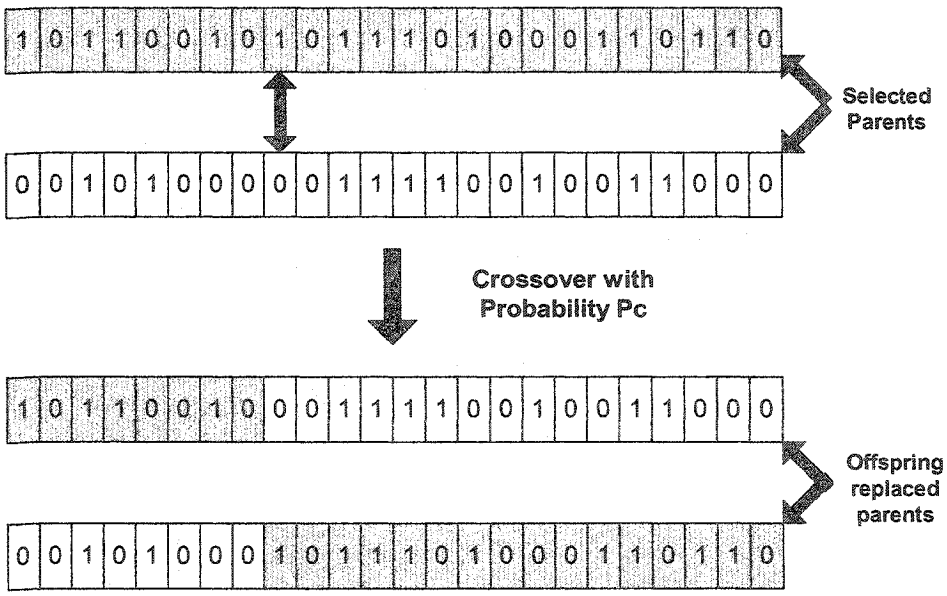

Fig 3.5 Diagram of crossover operation.

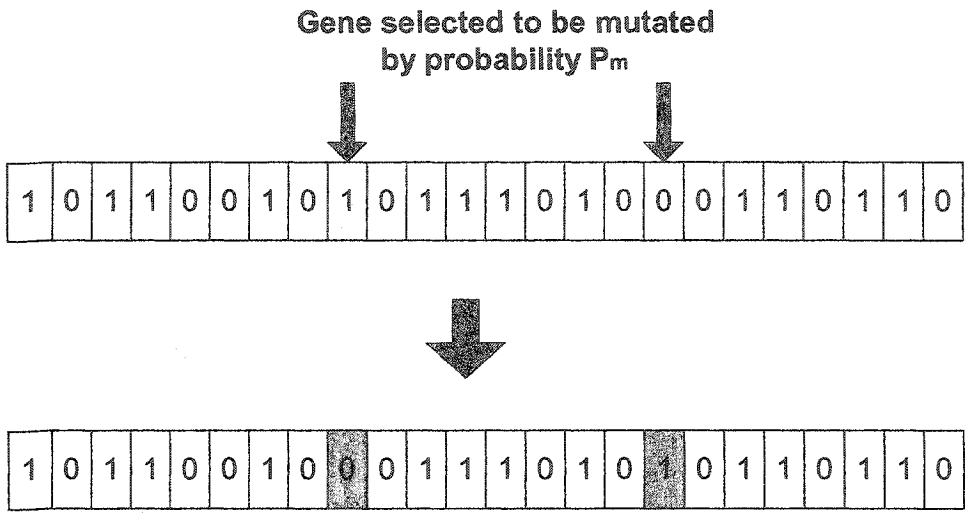

Fig 3.6 Diagram of mutation operation.

In this thesis, crossover probability P_c and mutation probability P_m are empirically chosen to be 0.4 and 0.002, respectively.

Finally, replace the old population by the new temporary generation. Increase the generation counter by 1 and repeat from step 2 until G generations preset have elapsed or the specifications are satisfied.

3. 2 Design examples

Two design examples under ideal condition and non-ideal conditions are considered in this section.

3. 2. 1 Design under ideal condition

Based on the theory model presented in Chapter 2, the design problem has been reduced to find the coefficients, or the reflectivities $\{R_k\}$ of the FBG array, with specifications given by $f_{pass}T = 0.15$, $A_{pass} \pm \delta_1 = 0 \pm 2dB$, $f_{stop}T = 0.35$ and $\delta_2 = -20dB$.

We start the GA algorithms from five taps (M=4) with uniform intervals and the given specifications are satisfied when number of taps reaches 10 (M=9). The simulated filter response is shown in Fig 3.7 with the specifications indicated in the figure. To achieve the specifications, the filter coefficients are $\{R_k\} = \{0.1843, 0.4431, 0.3765, 0.0902, 0, 0, 0, 0, 0.0275, 0.0196\}$. Note that the genetic algorithms generated a family of solutions; each of them can meet the desired specifications. The reason why this solution is selected is that only six FBGs are actually needed in this design, since the coefficients for R_4, R_5, R_6, R_7 are equal to zero. Fig 3.8 shows the best and average fitness in population as a function of generation g. The GA parameters used in the design are also shown in this figure. The fitness is obtained by sampling 100 points evenly over the pass-band and stop-band and inverting their weighted maximum error. These operations are expressed by Eq. (3.5), Eq. (3.6) and Eq.

(3.8). The larger the fitness is, the better approximation to the desired transfer function is produced.

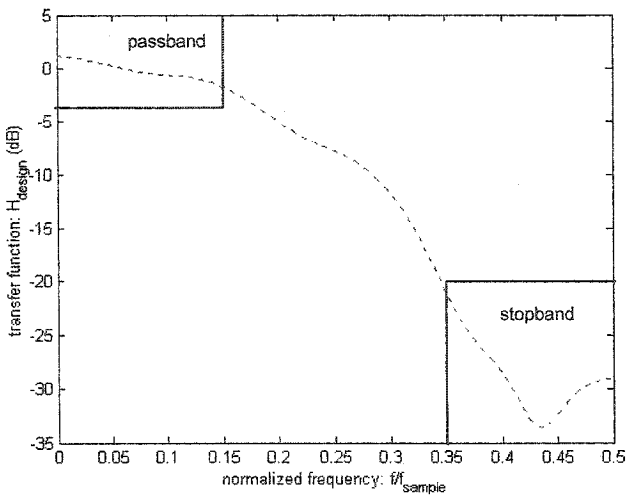

Fig 3.7 Filter response: nine taps with coefficients $\{R_n\} = \{0.1843, 0.4431, 0.3765, 0.0902, 0, 0, 0, 0, 0.0275, 0.0196\}$.

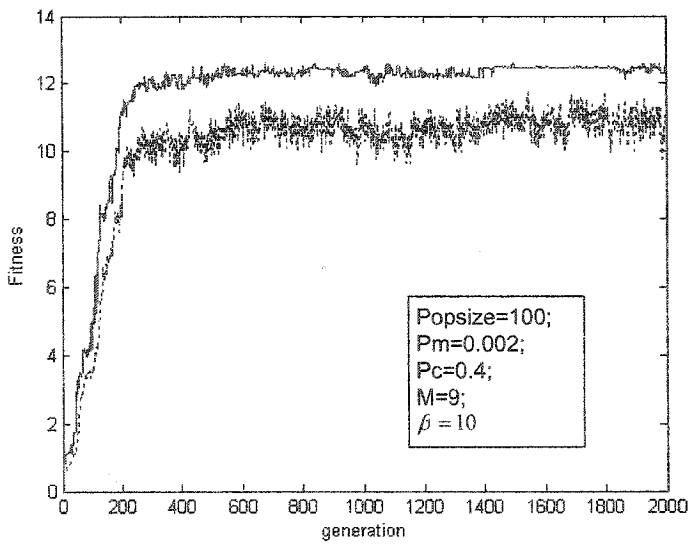

Fig 3.8 Best (solid) and average fitness (dotted) as the function of generation.

3. 2. 2 Design under non-ideal condition

In real system implementation, the following issues should be addressed carefully.

First, it is very difficult to fabricate FBGs with peak reflectivities less than 0.1. Although in theory it is possible, the accuracy cannot be guaranteed. Usually, reflectivity greater than 0.1 is practical in real implementation. With genetic algorithms, one may simply specify a low bound to R_k and this problem can be easily solved. In our design, we set $0.1 < R_k < 1.0$.

Second, the power spectrum of the broadband light source is not as flat as we expected, this is another important issue that cannot be ignored. As can be seen in Fig 3.9, the modulated optical power spectrum is a function of wavelength λ, which is determined by the power spectrum of the light source, and it is usually not flat. Two methods can be used to solve this problem. One is to apply an optical gain equalizer to flatten the power spectrum. But, this will increase the complexity and instability of the whole system. Another method is to introduce weighting coefficients $\{W_k\}$ according to the power spectrum incident into this FBG array to calibrate the reflectivities.

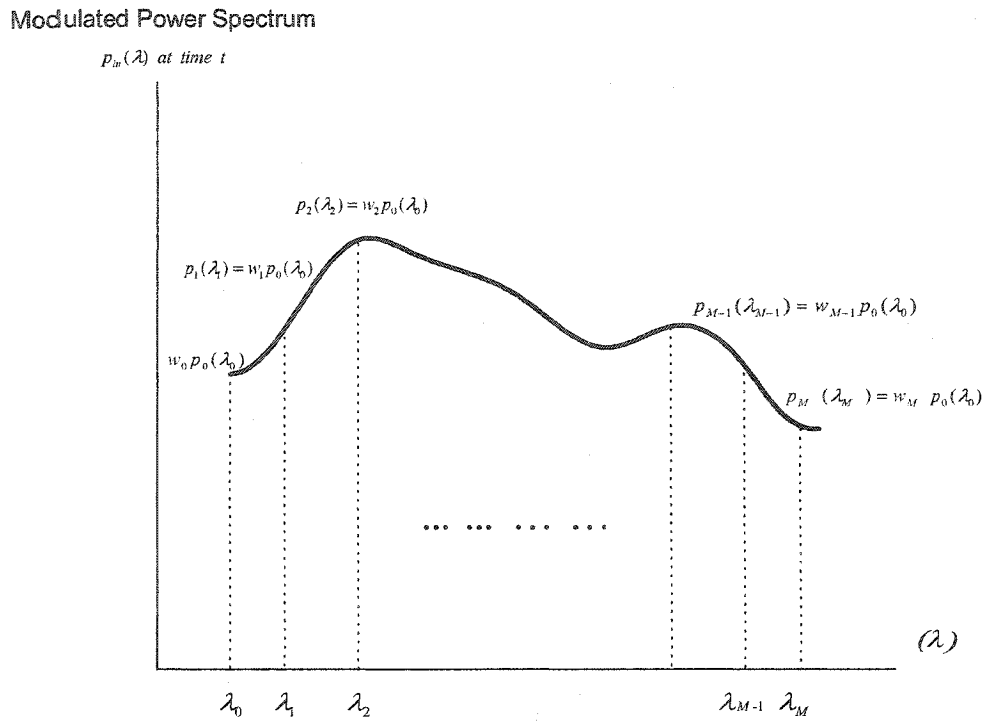

Fig 3.9 Calibration for the optical power spectrum of the modulated light.

We can see that the effective input optical power intensity is

$$P_{in} = [\int_{\lambda_0,\Delta\lambda} p_0(\lambda_0)d\lambda + \int_{\lambda_1,\Delta\lambda} p_1(\lambda_1)d\lambda + \cdots + \int_{\lambda_M,\Delta\lambda} p_M(\lambda_M)d\lambda] \cdot \frac{[1+mx(t)]}{2}$$

$$= [\int_{\lambda_0,\Delta\lambda} W_0 p_0(\lambda_0)d\lambda + \int_{\lambda_1,\Delta\lambda} W_1 p_0(\lambda_0)d\lambda + \cdots + \int_{\lambda_M,\Delta\lambda} W_M p_0(\lambda_0)d\lambda] \cdot \frac{[1+mx(t)]}{2}, \quad (3.9)$$

where $W_k \equiv p_k(\lambda_k)/p_0(\lambda_0)$, so $W_0 = 1$.

Again, use the assumption in Eq. (2.27) and define $p_0(\lambda_0) = p$, Eq. (3.9) can be approximately expressed as

$$\mathrm{P}_{in}(t) = (\sum_{k=0}^{M} W_k) \cdot p \cdot \Delta\lambda . \tag{3.10}$$

Similar to Eq. (2.29), the ac component at the photodetector output is

$$y(t) \propto \sum_{k=0}^{M} R_k W_k x(t - kT) . \tag{3.11}$$

Applying Fourier transform to both sides of Eq. (3.11), we obtain the system transform function of the filter:

$$H_{design}(\omega) = K' \sum_{k=0}^{M} R'_k e^{-j\omega kT} , \tag{3.12}$$

where $\{R'_k = W_k R_k\}$ with $k = 0,1,...,M$ is the effective coefficients, and K' is a scaling factor.

Third, from the simulation results obtained under the ideal conditions we find that zero coefficients occur. This indicates that by modifying the algorithm

through choosing variable tapping intervals instead of uniform tapping interval, the performance of the all-optical microwave filter would be improved. To achieve this, a minimum interval τ is defined, then the real tapping intervals T_n can be set as the integer times of τ, that is

$$T_k = q_k \cdot \tau;, \tag{3.13}$$

where q_k is non-negative integer number, with $k = 0,1,2,\cdots,M$; and when $k = 0$, $T_0 = q_0\tau = 0$.

Consequently, a second sequence of variables $\{q_1, q_2, \cdots, q_{N-1}\}$ is introduced into the algorithm. The revised system transform function can now be written as

$$H_{design}(\omega) = \sum_{k=0}^{M} R'_k e^{-j\omega k\tau \sum_{n=0}^{k} q_k} . \tag{3.14}$$

In Eq. (3.14), the factor K' is set to one. Since K' is only a scaling factor of the system function H_{design}, setting it to one will not affect the response of the filter.

The solution can now be expressed as $\{R_0, R_1, ..., R_M; \lambda_0, \lambda_1, \cdots, \lambda_M; q_1, q_2, \cdots, q_M; W_1, W_2, \cdots, W_M\}$, where λ_k and W_k are used to calculate R_k from R'_k, by considering un-flat power spectrum of the incident light. The power spectrum calibration for the non-flat modulated light is shown in Fig 3.9.

Fig 3.10 shows the filter transfer function when non-uniform tapping intervals are employed in the design. It can be seen by comparing Fig 3.7 and Fig 3.10, the design specifications are satisfied when the tapping intervals are uniform and variable. For the design with non-uniform tapping intervals, the same number of FBGs is required, but the FBG reflectivities are all within the range from 0.1 to 1. The fitness compared to the one with uniform tapping intervals is a little poorer (from Fig 3.10 we can see the response has more ripples), but the expected specifications are still well met. Fig 3.11 shows the best and average fitness in population as a function of generation g. The GA parameters used in the second example are also shown in this figure.

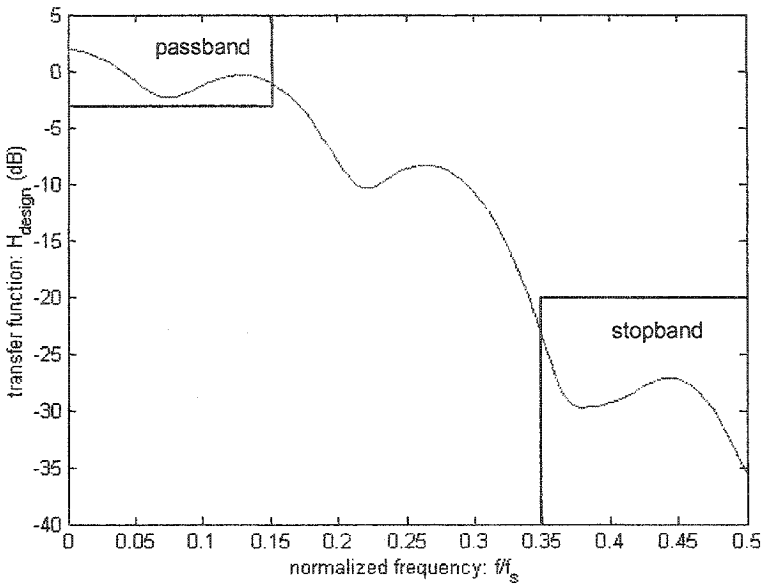

Fig 3.10 Filter design: six taps with coefficients: $\{R_k\} = \{0.1000, 0.3224, 0.4282, 0.2129, 0.1000, 0.1000\}$; $\{q_k\} = \{1.00, 1.00, 1.00, 5.00, 1.00\}$.

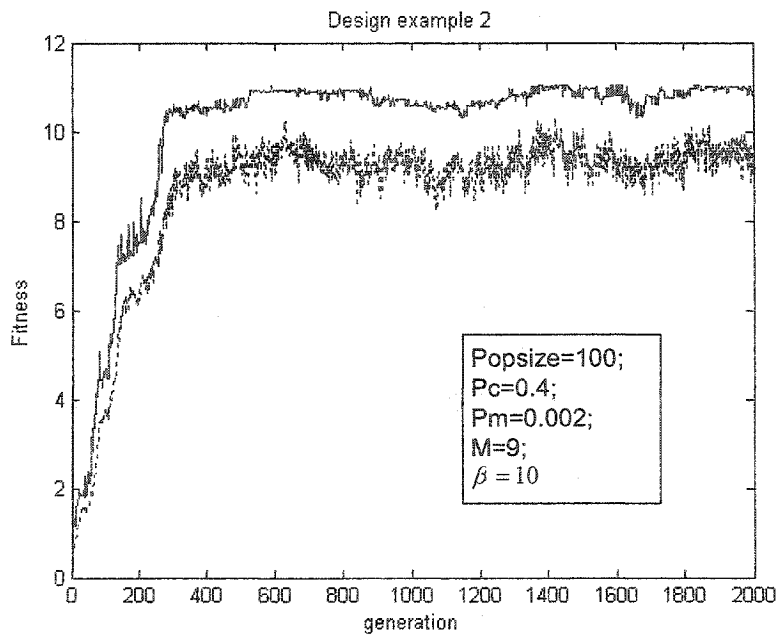

Fig 3.11 Best (solid) and average fitness (dotted) as the function of generation.

3.3 Further discussion

Note that in the design of the all-optical microwave filters, the coefficients are constraint with positive values due to the incoherent interference, which prevents the inclusion of negative coefficients. However, using differential detection technique, coefficients with negative values are possible. One example is shown in Fig 3.12. We distribute the positive coefficients and negative coefficients on two arms of the FBG delay lines according to the design results. The time-delayed light beams are then applied to two photodetectors with differential detection. Then the negative filter coefficients can be achieved. Compared with the structure provided in Ref. 65, this method is obviously easier and requires much less connectors; therefore, better performance with higher reliability can be provided.

It is believed that with negative coefficients, to meet the same specifications, less taps are required. One design example with only six taps (M=5) is obtained by setting $-1 < R_k < 1$. Its transfer function is shown in Fig. 3.13. We can see that the given design specifications are well satisfied by only using 6 taps when negative coefficients are available. In addition, band-pass or high-pass filters can also be designed and implemented if filter coefficients can be negative values.

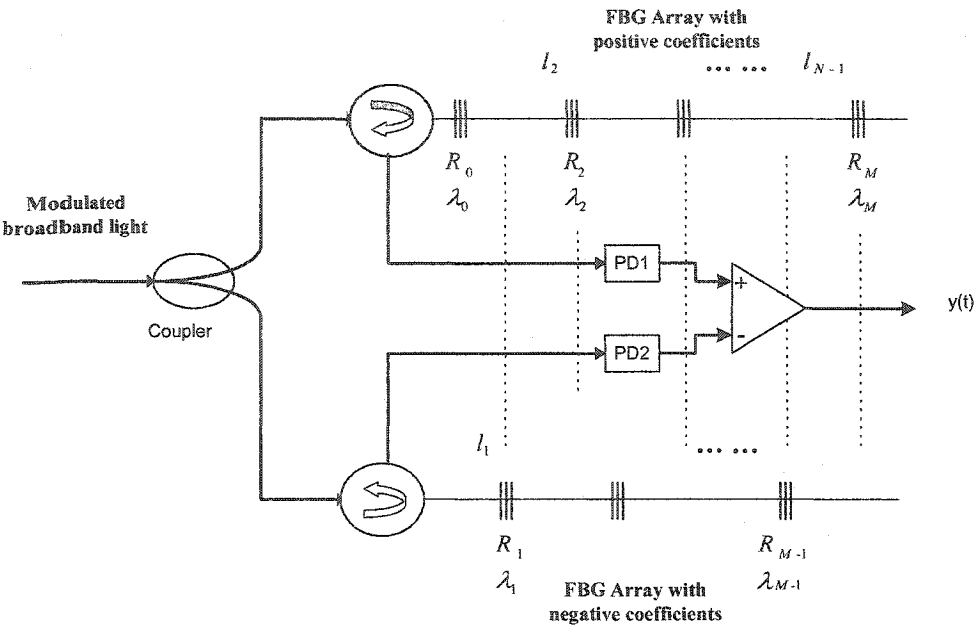

Fig 3.12 Diagram of optical microwave filter with negative coefficients

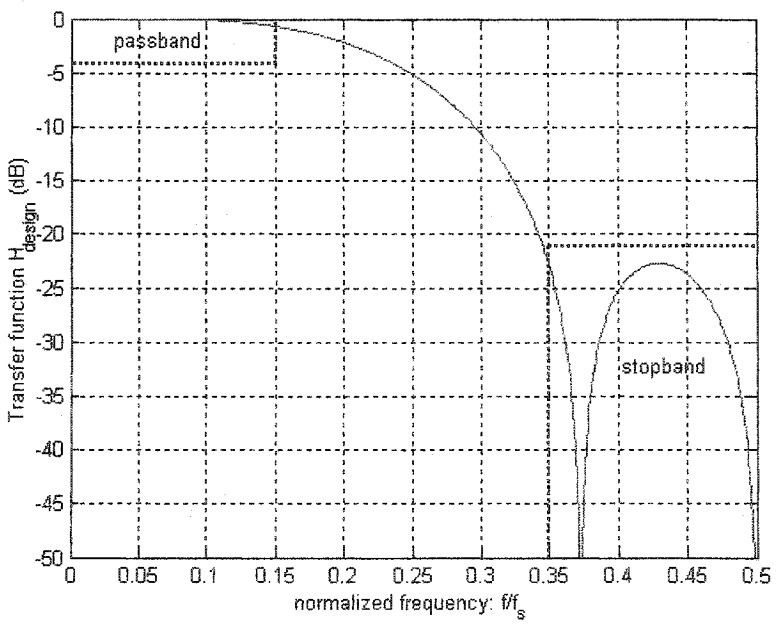

Fig 3.13 Low-pass filter with uniform tap intervals and negative coefficients:

$\{R_k\} = \{-0.07, 0.125, 0.463, 0.463, 0.125, -0.07\}$.

3.4 Summary

The synthesis of all-optical microwave filters using genetic algorithms has been presented in this chapter. The algorithms developed could be used to design FBG-based all-optical microwave filters with fixed or variable tapping intervals. Compared to the all-optical microwave filters using directional couplers or Mach-Zehnder lattices, FBG-based all-optical microwave filters have the advantages of reconfigurability and scalability with much simpler structure. The proposed algorithms can also be used to design all-optical microwave filters with negative coefficients when differential detection is applied, which make the design feasible for all types of filters.

Chapter 4

FILTER IMPLEMENTATION

Based on the two deign examples presented in Chapter 3, two FBG arrays are fabricated. The FBGs are fabricated using UV photo-imprinting technique with phase masks. The microwave filters using the fabricated FBG arrays are constructed and their performance is characterized and analyzed.

4. 1 FBG fabrication

The FBGs are fabricated at Bragg Photonics Inc at Montréal using UV photo-imprinting technique with phase masks [80-83]. The schematic of fabrication process is illustrated in Fig 4.1.

Phase mask (PM) is one of the key components for FBG fabrication. The period of the phase mask determines the center wavelength of the fabricated FBG. Phase masks are usually made from a flat slab of silica glass which is transparent to UV light. On one of the slab surface, a one-dimensional periodic surface relief structure is etched by using photolithographic techniques. The shape of this periodic pattern approximates a square wave in profile.

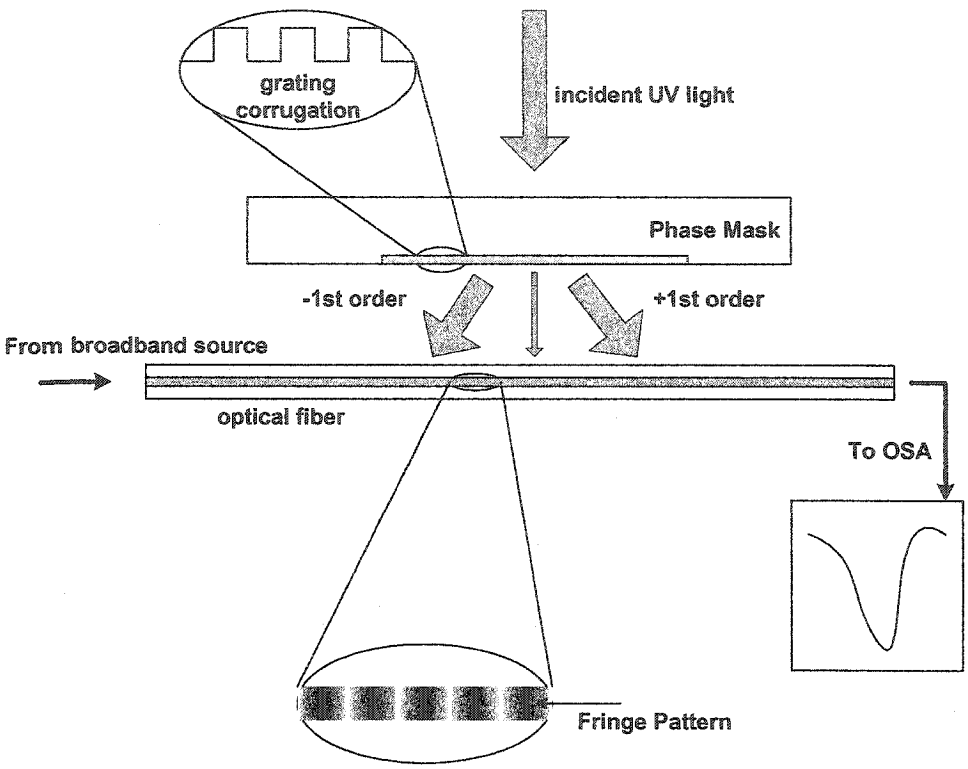

Fig 4.1 Bragg grating fabrication apparatus based on a null-zero-order diffraction phase mask.

A KrF (248 nm) excimer laser is used to illuminate the phase mask. Because the depth of the corrugations of the phase mask is designed to reduce the light transmitted in the zero-order beam to less than 5% of the total throughput while more than 75% of the throughput being in the ± 1 diffracted beams. The two ± 1 order diffracted beams interfere to produce a periodic pattern that photoimprinting out a corresponding grating in the photosensitive fiber. If the period of the phase mask is Λ_{PM}, the period of the grating is $\Lambda_{PM}/2$. An

FBG array consists of numbers of uniform FBGs distributed along the length of the fiber. Each FBG has a different Bragg wavelength, which requires different phase mask. To ensure a proper reflectivity and exact center reflection wavelength, a broadband light source and an optical spectrum analyzer (OSA) are used to monitor the transmission spectrum during the inscription process. By controlling the output intensity and exposed time of the UV light, the desired reflectivity and bandwidth can be achieved. The exact center wavelength for the FBG is adjusted by applying a tension controller to the pigtail of the fiber. The grating period will change when the fiber is released from the holder.

4. 2 Experiments

The experiments are carried out based on the two FBG arrays fabricated. The performance of the two filters are measured and further analyzed.

4. 2. 1 Filter transfer function – design example 1

One FBG array (Array 1) is fabricated based on the design example 1, where the effective coefficients are not calibrated. The FBG array is fabricated following the following steps:

1) Translate the design coefficients to the fabrication parameters

In design example 1, no calibration is employed for the effective coefficients. The objective values of the peak transmission power for each FBG in the FBG array, in dB, are directly derived from the design results $\{R_k\} = \{0.1843, 0.4431, 0.3765, 0.0902, 0, 0, 0, 0, 0.0275, 0.0196\}$ by using the equation

$$\mathrm{T}_k = -10\log_{10}(1 - R_k \cdot 100\%), \tag{4.1}$$

where T_k is the peak power transmission ratio in dB of the k-th FBG, and $R_k \cdot 100\%$ is the peak reflectivity in percent.

2) Fabrication of FBGs with small reflectivities

We see that three FBGs have reflectivities less than 10%, two of them with reflectivities even smaller, 2~3%. In order to obtain these small reflectivities, a very slow fabrication process with low UV illumination is required. In practice, a simpler and more effective way get fabricate weak gratings is to reduce the length of the FBGs. Therefore, a 4-mm slit is employed before the phase mask to limit the length of fiber that is illuminated by the UV light. For

FBGs with higher reflectivities, a 10-mm-wide UV beam is used directly to illuminate the PM.

3) Thermal decay

Since the FBGs are written in hydrogen-loaded single mode fiber, thermal decay will result in slight center wavelength shift and peak reflectivity degradation, which occurs over time, even at room temperature [82]. Before the measurement of the filter response, the characteristics of the FBGs, including the central wavelength, full width at half maximum (FWHM) bandwidth and peak reflectivity, are re-measured. Due to the thermal decay, the measured parameters are slightly different from what we obtained during the FBG fabrication process. In the following analysis, the theoretical filter frequency responses are based on the re-measured FBG characteristics. In real applications, it is essential to use non-hydrogen loaded FBG or pre-annealed hydrogen loaded FBG to eliminate the thermal decay effects.

The characteristics of the FBG array are summarized in Table 4.1. The center wavelength of each FBG is determined by the phase mask used to produce the FBG. The spacing of center wavelengths between any adjacent FBGs is about 3 ~ 4 nm, which is large enough to avoid cross interference between the

reflected signals. The peak reflectivities are obtained from the transmission spectrum (shown in Fig 4.2) and calculated using Eq. (4.1). From Table 4.1, we can see that although methods have been taken to ensure the accuracy of the FBGs with small reflectivities, reflectivity errors still exist. To avoid these errors, weak FBGs should be avoided in the filter design.

Table 4.1 Characteristics of FBG array 1.

No. of FBG	Center wavelength (nm)	3dB bandwidth (nm)	Peak reflectivity (%)	Grating length (mm)	Grating spacing (mm)
#1	1538.63	0.11	15.02	10	———
#2	1542.47	0.12	38.24	10	100
#3	1546.20	0.12	32.49	10	100
#4	1549.74	0.19	8.23	4	100
#5	1552.53	0.19	4.08	4	500
#6	1555.93	0.19	3.55	4	100

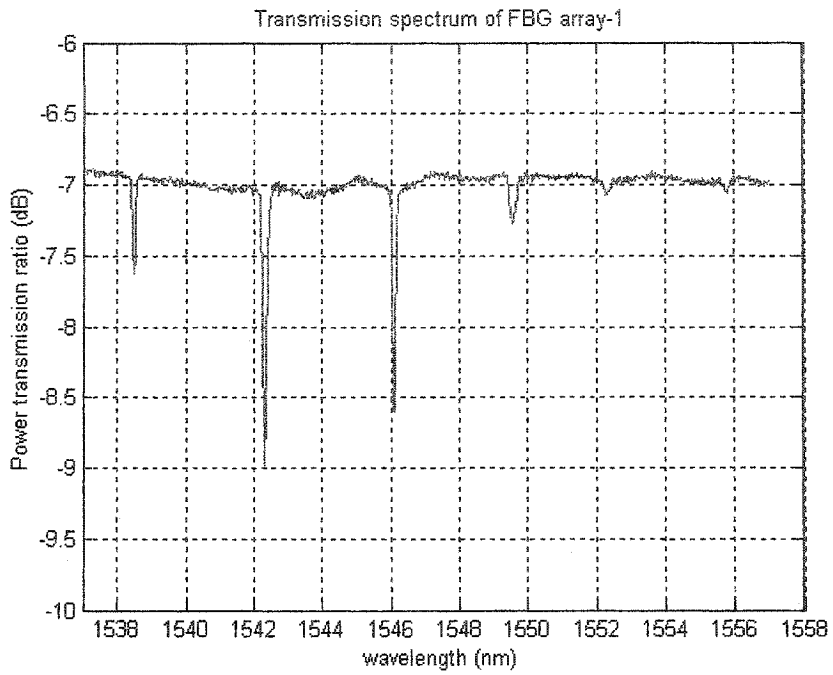

Fig 4.2 Transmission spectrum of FBG Array 1.

The experimental setup is shown in Fig 4.3. An erbium-doped fiber amplifier (EDFA) is used as the broadband optical source, followed by a polarization controller (PC) to control the polarization state of the light incident into the modulator. The polarization-optimized broadband light is then intensity modulated by the EOM and fed to the FBG array via an optical circulator. A second EDFA is employed before the circulator to compensate for the power loss in the system. The reflected time-delayed signals are summed at the photodetector. The microwave signal is generated using an Agilent PSG-A series signal generator (E8254A). An Agilent PSA series spectrum analyzer (E4448A) is used to monitor the microwave signal.

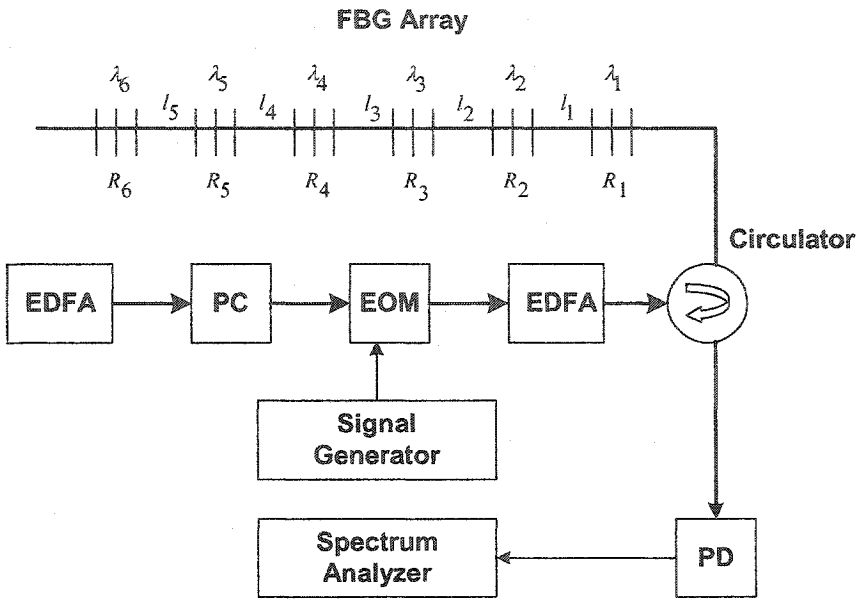

Fig 4.3 Experimental setup of the FBG based all-optical microwave filter.

The adjacent grating spacing of the FBG array is 10 cm, which corresponds to a basic time delay of 0.966 ns. The spectral period of the filter is 1.036 GHz, calculated based on Eq. (2.26). By tuning the RF signal from 0 to 1.1 GHz while keeping the amplitude constant, we obtain the filter magnitude response. Fig 4.4 shows the magnitude responses obtained from the experiment and the simulation using the coefficients listed as the peak reflectivities in Table 4.1, {0.1520, 0.3824, 0.3249, 0.0823, 0, 0, 0, 0, 0.0408, 0.0355}, which is obtained from the transmission spectrum (shown in Fig 4.2). It can be seen that these two responses do not match well. The reason of the difference is that the power spectrum of the modulated light incident into the FBG array is not flat as can be seen in Fig 4.5 (a).

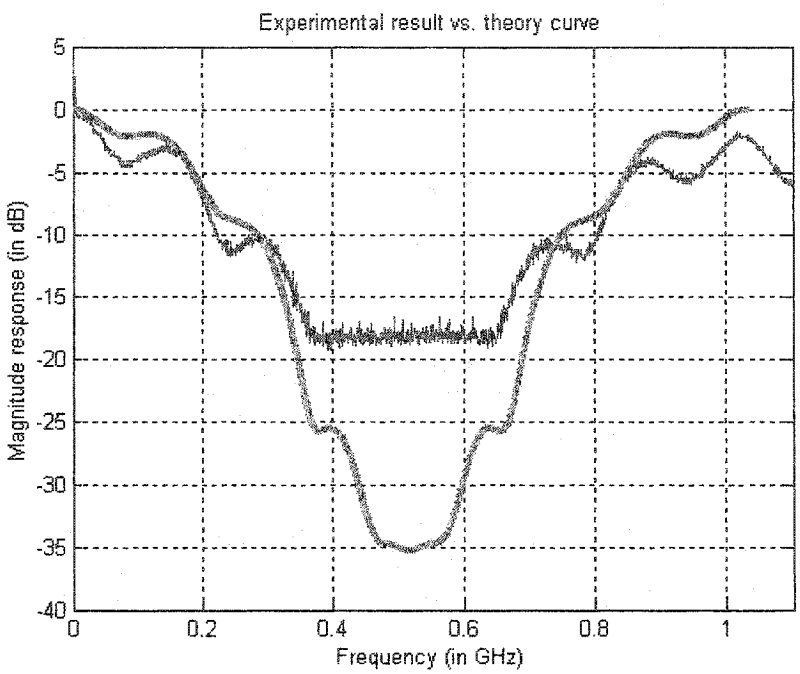

Fig 4.4 Filter magnitude responses: experimental (dark) and theoretical (grey).

The real reflected spectrum of FBG Array 1 is shown in Fig 4.5 (b). Using the effective coefficients {1.0000, 3.7119, 5.8695, 1.9884, 0, 0, 0, 0, 0.8316, 0.9080}, which are calculated from the peak reflectivities in the real reflected spectrum, a good agreement between the experimental results and the theoretical calculations is obtained, as can be seen in Fig 4.6. We may notice that the experimental stop-band response does not match well with the theoretical response. This mismatch is caused by the limited dynamic range of the spectrum analyzer.

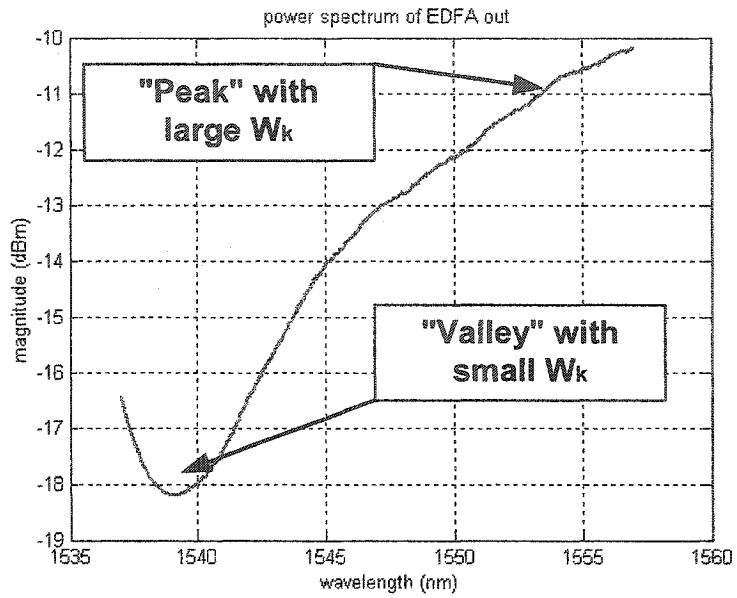

(a)

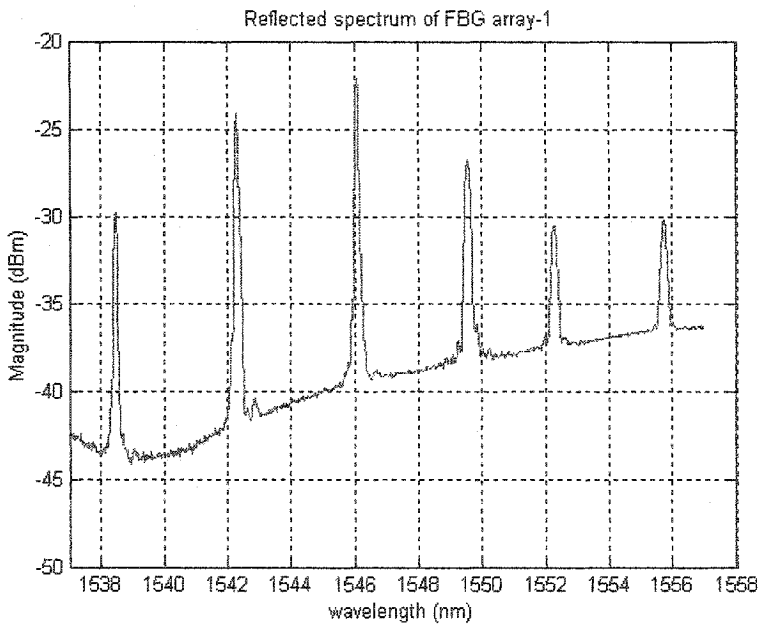

(b)

Fig 4.5 (a) Power spectrum of the EDFA (b) Reflected power spectrum of FBG Array 1

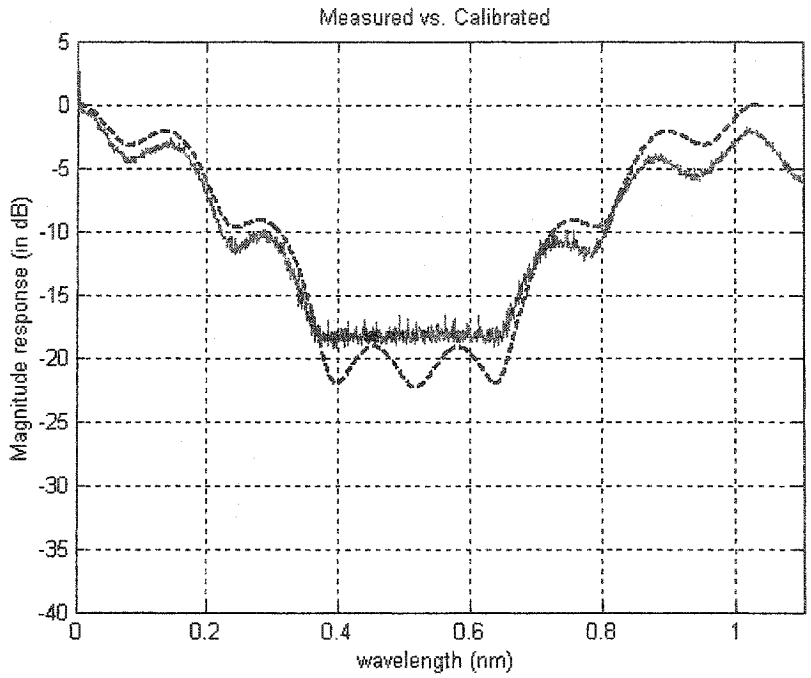

Fig 4.6 Filter magnitude responses: experimental (solid) and theoretical with calibration (dashed).

Comparing Fig 4.4 and Fig 4.6, we conclude that 1) calibrating the effective coefficients is necessary when the broadband light source is not flat and 2) acceptable agreement between simulation and experimental results is achieved by calibrating the effective coefficients based on the peak reflectivities in the real reflected spectrum.

4. 2. 2 Filter transfer function - design example 2

The following measures have been taken in the fabrication of FBG Array 2:

1) Calibrating the un-flat power spectrum of the modulated light

The weighting sequence $\{W_k\}$, {1, 1.22, 1.93, 2.02, 0, 0, 0, 0, 2.55, 2.69}, is calculated from the EDFA power spectrum shown in Fig 4.5 (a). Based on Eq. (3.11), the desired reflectivities of the FBGs in the FBG array is calibrated to be

$\{R_k\} = \{R'_k\}/\{W_k\} = \{0.1, 0.2643, 0.2219, 0.1054, 0, 0, 0, 0, 0.0392, 0.0372\}$,

where $\{R'_k\}$ are the effective coefficients.

2) Avoiding using weak FBGs to reduce implementation error

To avoid using weak FBGs with reflectivities less than 10%, in the design we increase $\{R_k\}$ to a higher level by multiplying $\{R_k\}$ with a constant greater than one. In this example, multiplying 3.45 to $\{R_k\}$ leads to new reflectivities of {0.345, 0.912, 0.765, 0.365, 0, 0, 0, 0, 0.135, 0.129}. Of course, the maximum reflectivity in the coefficients can be normalized to unity if FBGs

with 100% reflectivity can be fabricated. Normalizing the coefficients will increase the magnitude of the filter response while keeping the response shape unchanged. With this operation, all the FBGs will have reflectivities greater than 10%.

Weak FBGs can also be avoided if the FBGs with small reflectivities are located at or near the "valley" of the incident power spectrum by properly selecting their center wavelengths, as can be seen in Fig 4.5 (a). Since $\{R_k\} = \{R'_k\} / \{W_k\}$, small weights W_k result in large reflectivities R_k.

The two methods can also be combined to achieve even better results. For FBGs with small reflectivity variations, we can use the same fabrication conditions. For example, the UV illumination intensity can be constant for all the FBGs, which could ensure a uniform quality for the FBGs.

The characteristics of FBG Array 2 are summarized in Table 4.2. The listed peak reflectivities are calculated from the measured transmission spectrum which is shown in Fig 4.7 (a). Both the normalized peak reflectivities and the normalized power reflectivities are based on the reflection spectrum of FBG Array 2, which is shown in Fig 4.7 (b). The normalized peak reflectivities are calculated from the peak values of each FBG, while the normalized power

reflectivities are obtained by integrating the reflected power within the 10 dB-bandwidth of the FBGs.

Table 4.2 Characteristics of FBG Array 2.

No. of FBG	Center wavelength (nm)	3dB bandwidth (nm)	Peak reflectivity (%)	Normalized peak reflectivity	Normalized power reflectivity	Grating length (mm)	Grating spacing (mm)
#1	1538.54	0.12	30.08	0.2016	0.2016	10	———
#2	1542.46	0.20	85.42	0.9345	1.4715	10	100
#3	1546.17	0.16	69.35	1.4210	1.6759	10	100
#4	1549.70	0.12	31.13	0.8517	0.7421	10	100
#5	1552.55	0.10	11.77	0.4170	0.3136	10	500
#6	1555.82	0.10	11.45	0.4751	0.3752	10	100

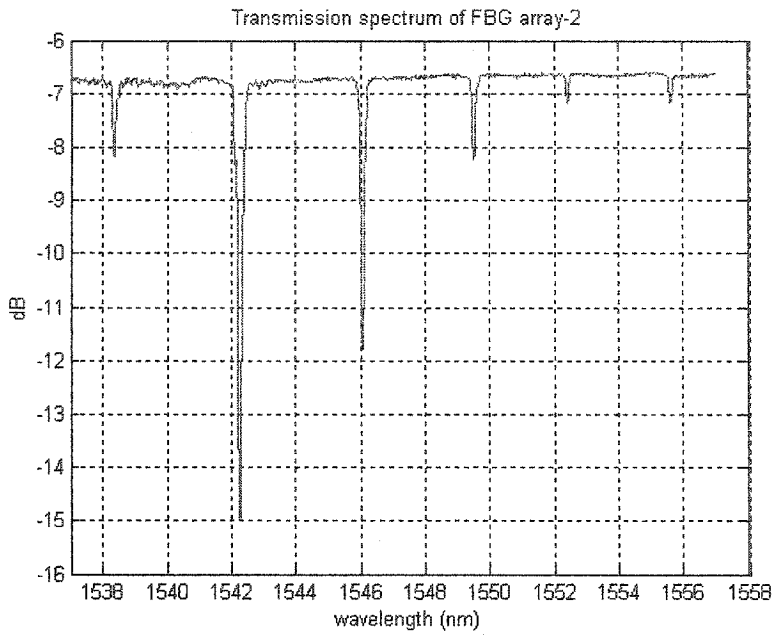

(a)

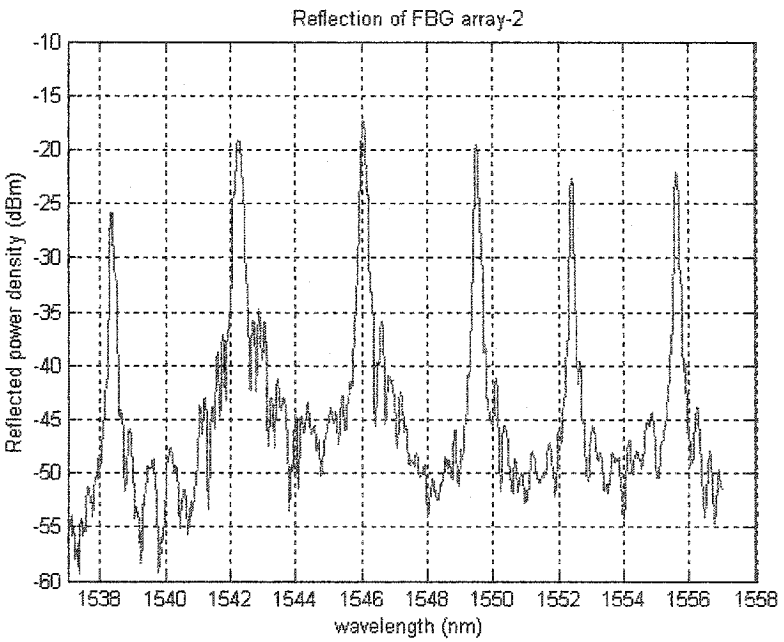

(b)

Fig 4.7 (a)Transmission spectrum and (b)Reflection spectrum of FBG Array 2.

Three filter magnitude responses are plotted in Fig 4.8, including 1) the measured system transfer function, 2) the calculated filter magnitude response based on the normalized peak reflectivities listed in Table 4.2, and 3) the calculated filter magnitude response based on the normalized power reflectivities listed in Table 4.2. It can be clearly seen that the simulation based on the normalized power reflectivities shows a better agreement with the experimental result than the calculated filter response based on the normalized peak reflectivities. The reason that the power reflectivities are more accurate than the peak reflectivities is that the bandwidths of the FBGs are taken into account in calculating the power reflectivities, while in calculating the peak reflectivities, we assume that all FBGs have identical bandwidths. In fact, FBG bandwidth is dependent on FBG fabrication parameters, including the length of the FBG and the depth of refractive index change. A discussion can be found in Section 2.2.1.

Based on the normalized power reflectivities, the effective coefficients can be expressed as

$$R'_k = \frac{\int_{\lambda_k,\Delta\lambda_k} p(\lambda)\cdot R_k(\lambda)d\lambda}{\int_{\lambda_k,\Delta\lambda_0} p(\lambda)\cdot R_0(\lambda)d\lambda} = \frac{\int_{\lambda_k,\Delta\lambda_k} p(\lambda)d\lambda \cdot \int_{\lambda_k,\Delta\lambda_k} R_k(\lambda)d\lambda}{\int_{\lambda_k,\Delta\lambda_0} p(\lambda)d\lambda \cdot \int_{\lambda_k,\Delta\lambda_0} R_0(\lambda)d\lambda}, \tag{4.2}$$

where the dominator denotes the reflected power of the first FBG in the FBG

array, and the nominator represents the reflected power of the k-th FBG. In Eq. (4.2), R'_k is obtained during the design using the genetic algorithm; $\int_{\lambda_0,\Delta\lambda_0} p(\lambda)d\lambda \cdot \int_{\lambda_0,\Delta\lambda_0} R_0(\lambda)d\lambda$ can be properly determined during the FBG writing process, and $\int_{\lambda_k,\Delta\lambda_k} p(\lambda)d\lambda$ can be calculated from the power spectrum of the incident light. Then the fabrication objective becomes to monitor the reflected power at the k-th FBG $\int_{\lambda_k,\Delta\lambda_k} R_k(\lambda)d\lambda$. This result indicates that it is more accurate to monitor the reflected power by using an optical power meter than observing the transmission power spectrum using an OSA during the FBG fabrication process.

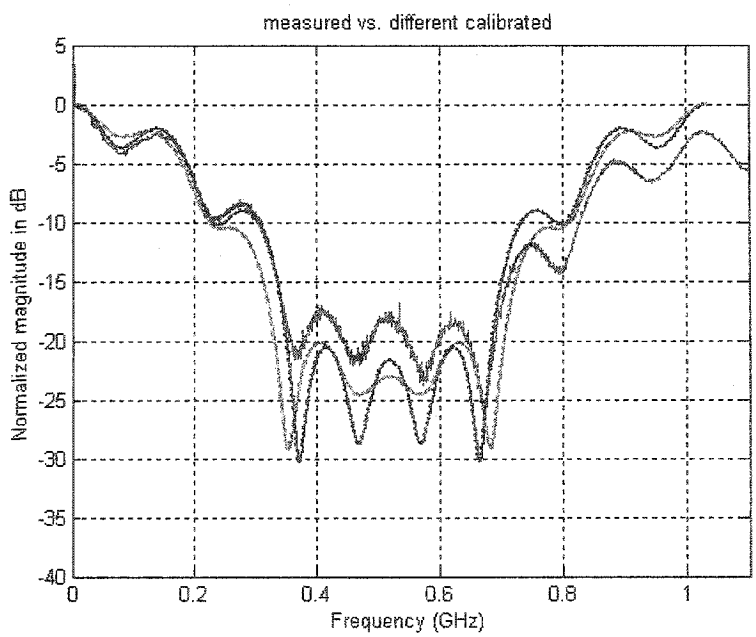

Fig 4.8 Experimental (solid), reflection-peak calibrated (dashed) and reflection-power calibrated (dotted) magnitude responses.

In practice, all the FBGs in the FBG array are fabricated in one fiber. If an optical power meter is used to measure the reflected power of the FBG array, it measures the power reflected by all the FBGs. Then the power reflected by the k'th FBG is calculated using the following equation,

$$P_k = \frac{R'_k \cdot P_0}{\int_{\lambda_k, \Delta\lambda_k} p(\lambda) d\lambda} + P_{k-1}, \tag{4.3}$$

where P_0 is the reflected power measured after the first FBG is fabricated, and P_{k-1} is the total reflected power measured after the $k-1$'th grating is fabricated.

4.3 Summary

Two FBG arrays were fabricated based on the design using genetic algorithms. Experiments have been carried out using the two FBG arrays. Implementation issues have been raised and discussed. The experimental results showed that the filter coefficients must be calibrated to get a filter response identical to the theoretical design. To calibrate the filter coefficients, the un-flat power

spectrum of the broadband light source and bandwidths of the FBGs must be considered.

To avoid fabrication errors, weak gratings should be avoided in the filter design. Two methods have been proposed, by either normalizing the FBG reflectivities, or carefully locating the wavelengths of the FBGs to achieve relatively uniform reflectivities, to solve this problem.

Chapter 5

DISPERSION EFFECTS

In the above discussions, all FBGs are assumed to have identical time delay for all the frequency components of the incident light. However, if the modulated light is reflected by an FBG, different spectral components will experience different phase shifts depending on the FBG synthesis parameters and the modulation frequency [84-92], chromatic dispersion is generated. These phase shifts result in relative phase differences between the carrier and the sidebands, which finally lead to power degradation and an unexpected phase shift of the recovered microwave signal at the photodetector. As can be seen in Fig 4.6 and Fig 4.8, where the filter response degrades when the modulating frequency increase. This is caused by the limited frequency response of the EOM and the photodetector. We will show in this chapter that dispersion effects will also lead to this degradation.

In this chapter, we will analyze and discuss the dispersion effects caused by the FBGs on the performance of the all-optical microwave filters. We will show that the dispersion effects will lead to power degradation. The degradation can be reduced by carefully selecting the FBG synthesis

parameters. We also show that the dispersion effects can be further reduced or almost eliminated if single sideband (SSB) modulation [88-92] scheme is employed.

5.1 Power spectrum of intensity modulated light

A broadband light source can be modeled as a large sum of light with different wavelengths over the range from λ_0 to λ_M; and each frequency component is incoherent with each other, which means the phase of each component can be treated as a independent random variable distributed uniformly over $-\pi$ to π. Mathematically, the optical electric field can be expressed as

$$E_{bs}(t) = \sum_k E_k e^{-j(\omega_k t + \varphi_k)}, \tag{5.1}$$

where E_{bs} denotes the electric field of the broadband optical source; E_k is the electric field amplitude for the k-th frequency component, ω_k is the k-th angular frequency which can also be written as $\omega_k = 2\pi c / \lambda_k$, and φ_k is the random phase for the k-th frequency component.

When this broadband light source is intensity modulated (IM) by an external electro-optic modulator, the normalized complex amplitude of the electric field may be expressed as

$$E_{\text{mod}} = \sqrt{1 + m_{i,k} \cos(\omega_m t)} \cdot \sum_k E_k \cdot e^{j(\omega_k t + \varphi_k)}, \tag{5.2}$$

where E_{mod} denotes the output electric field of the EOM, $m_{i,k}$ is the intensity modulation index for the k-th optical carrier, ω_m is the modulating angular frequency. Here we assume the initial phase of modulating RF signal is zero.

To determine the chromatic dispersion of the modulated signal, we will analyze the spectrum of the signal by expanding its amplitude term into Fourier series. In order to simplify the notations, E_0, ω_0, φ_0 and m_0 are used to replace $\{E_k\}$, $\{\omega_k\}$, $\{\varphi_k\}$ and $\{m_{i,k}\}$ respectively. That is

$$E_0(1 + m_0 \cos \omega_m t)^{1/2} = E_0(K_0 + K_1 \cos \omega_m t + K_2 \cos 2\omega_m t + \cdots), \tag{5.3}$$

where $K_0 = \frac{1}{T}\int_0^T (1 + m_0 \cos \omega_m t)^{1/2} dt$ and

$K_n = \frac{2}{T}\int_0^T (1 + m_0 \cos \omega_m t)^{1/2} \cdot \cos n\omega_m t \, dt$, n=1, 2... In Eq. (5.2), we assume

that the carrier components are incoherent with each other. For small value of m_0, the K_0 (dc) term is approximately unity, K_1 is approximately equal to $m_0/2$, and the higher order coefficients (harmonics) are very small. In fact, when m_0 increases, although the higher order harmonics increase more rapidly than term K_1, they are still very small. Under these conditions, higher order harmonics can be neglected and the amplitude modulation (AM) approximation of the IM is reasonable [84], that is

$$E_{\text{mod}}(t) = (1 + m_a \cos \omega_m t) \cdot E_0 \cdot e^{j(\omega_0 t + \varphi_0)}, \tag{5.4}$$

where m_a is normalized amplitude modulation index.

Applying Fourier transform to Eq. (5.4) we get the spectrum of $E_{\text{mod}}(t)$,

$$\begin{aligned} E_{\text{mod}}(\omega) &= E_0 \delta(\omega - \omega_0) e^{j\varphi_0} \\ &+ \frac{m_a}{2} E_0 \delta(\omega - \omega_0 - \omega_m) e^{j\varphi_0} + \frac{m_a}{2} E_0 \delta(\omega - \omega_0 + \omega_m) e^{j\varphi_0}. \end{aligned} \tag{5.5}$$

It consists of an optical carrier, an upper sideband (USB) and a lower sideband (LSB). The conventional AM is also called as double sideband (DSB) modulation.

5.2 Dispersion caused by a uniform FBG

When the intensity modulated light is launched into and reflected by the m-th (m=1, 2, 3, ..., M+1) uniform FBG in the FBG array, the three optical frequency components experience different phase delay. If we ignore the chromatic dispersion caused by the short length fiber jumpers in the system and only consider the phase shift induced by the FBG, we may get

$$\begin{aligned} E_{rfl}(t) &= E_0\rho_0\cos(\omega_0 t+\theta_0) \\ &+\frac{m_a}{2}E_0\cdot\rho_2\cos[(\omega-\omega_0-\omega_m)t+\theta_2]+\frac{m_a}{2}E_0\cdot\rho_1\cos[(\omega-\omega_0+\omega_m)t+\theta_1], \end{aligned} \tag{5.6}$$

where $\theta_0,\theta_1,\theta_2$, ρ_0,ρ_1,ρ_2 represent the phase shifts and amplitude reflection introduced by the FBG, with respect to frequency components $\omega_0,\omega_0-\omega_m,\omega_0+\omega_m$. $E_{rfl}(t)$ is the reflected optical electrical field.

The phase of a single optical frequency can be expressed as

$$\theta=\beta z, \tag{5.7}$$

where β is the propagation constant and z is the distance traveled. Expanding β in a Taylor series and substituting it into Eq. (5.7) yields

$$\theta = z\beta(\omega_0) + z\dot{\beta}(\omega_0)(\omega-\omega_0) + \frac{z}{2}\ddot{\beta}(\omega_0)(\omega-\omega_0)^2 + \frac{z}{6}\dddot{\beta}(\omega_0)(\omega-\omega_0)^3 + \frac{z}{24}\ddddot{\beta}(\omega_0)(\omega-\omega_0)^4 + \cdots, \tag{5.8}$$

where the $\dot{\beta}$, $\ddot{\beta}$, ..., are the first, second and higher-order derivatives with respect to the optical radian frequency, ω.

The group delay can also be expanded in a Taylor series,

$$T = z \cdot d\beta / d\omega = z[\dot{\beta}(\omega_0) + \ddot{\beta}(\omega_0)(\omega-\omega_0) + \frac{\dddot{\beta}}{2}(\omega_0)(\omega-\omega_0)^2 + \frac{\ddddot{\beta}}{6}(\omega_0)(\omega-\omega_0)^3 + \cdots]. \tag{5.9}$$

The first term $z\dot{\beta}(\omega_0)$ is a constant delay that does not alter or distort the optical signal.

Similarly, the first, second and third order dispersion are respectively written as the first, second and third order derivatives of the group delay

$$D = dT / d\omega = z \cdot \frac{d^2\beta}{d\omega^2}$$
$$= z[\ddot{\beta}(\omega_0) + \dddot{\beta}(\omega_0)(\omega - \omega_0) + \ddot{\beta}(\omega_0)(\omega - \omega_0)^2 + \cdots], \tag{5.10}$$

$$\dot{D} = z \cdot d^3\beta / d\omega^3 = z \cdot [\dddot{\beta}(\omega_0) + \ddot{\beta}(\omega_0)(\omega - \omega_0) + \cdots], \tag{5.11}$$

and

$$\ddot{D} = z \cdot d^4\beta / d\omega^4 = z \cdot \ddot{\beta}(\omega_0) + \cdots, \tag{5.12}$$

where higher order dispersion is neglected in present system application.

Using Eqs. (5.9) - (5.12), we get

$$\begin{cases} \ddot{\beta} = \dfrac{\ddot{D}}{z}; \\ \dddot{\beta} = \dfrac{\dot{D}}{z} - \dfrac{\ddot{D}}{z} \cdot (\omega - \omega_0); \\ \ddot{\beta} = \dfrac{D}{z} - \dfrac{\dot{D}}{z} \cdot (\omega - \omega_0) + \dfrac{3}{2} \cdot \dfrac{\ddot{D}}{z} \cdot (\omega - \omega_0)^2. \end{cases} \tag{5.13}$$

Substituting Eq. (5.12) into Eq. (5.8), the phase θ is

$$\theta = z\beta(\omega_0) + z\dot{\beta}(\omega_0)(\omega-\omega_0) + \frac{D}{2}(\omega-\omega_0)^2 - \frac{\dot{D}}{3}(\omega-\omega_0)^3 + \frac{5}{8}\cdot\ddot{D}(\omega-\omega_0)^4 + \cdots. \tag{5.14}$$

Evaluating θ at the reflected optical carrier and sidebands

$$\begin{cases} \theta_0 = z\beta(\omega_0); \\ \theta_1 = z\beta(\omega_0) - z\dot{\beta}(\omega_0)\omega_m + \frac{D}{2}\omega_m^2 - \frac{\dot{D}}{3}\omega_m{}^3 + \frac{5}{8}\cdot\ddot{D}\omega_m{}^4; \\ \theta_2 = z\beta(\omega_0) + z\dot{\beta}(\omega_0)\omega_m + \frac{D}{2}\omega_m^2 + \frac{\dot{D}}{3}\omega_m{}^3 + \frac{5}{8}\cdot\ddot{D}\omega_m{}^4. \end{cases} \tag{5.15}$$

Then the relationship between the phase shift and the group delay/dispersion of the FBG is built up. In the following sections, we will discuss the dispersion effects on the FBG-based microwave filters.

5.3 Detected signal at the photodetector

If the lightwave reaching the photodetector is given by Eq. (5.6) and Eq. (5.15), the photo current is obtained by using Eq. (2.13), discussed in Section 2.1.4. Taking only the RF signal centered at the modulation frequency ω_m and ignore the dc current and higher order harmonics, we get

$$y(t) = \frac{1}{2} m_a {E_0}^2 \rho_1 \rho_0 \cos(\omega_m t + \theta_0 - \theta_1) + \frac{1}{2} m_a {E_0}^2 \rho_2 \rho_0 \cos(\omega_m t + \theta_2 - \theta_0) . \quad (5.16)$$

Considering that

$$A\cos(\omega t + \phi_1) + B\cos(\omega t + \phi_2) = C\cos(\omega t + \phi_3), \quad (5.17)$$

where $C = \sqrt{A^2 + B^2 + 2AB\cos(\phi_2 - \phi_1)}$ and $\phi_3 = \tan^{-1}[\frac{A\sin\phi_1 + B\sin\phi_2}{A\cos\phi_1 + B\cos\phi_2}]$,

we have

$$y(t) = \frac{1}{2} m_a E_0^2 \rho_0 \sqrt{|\rho_1|^2 + |\rho_2|^2 + 2|\rho_1\rho_2|\cos(\theta_2 + \theta_1 - 2\theta_0)}\cos(\omega_m t + \theta_3), \quad (5.18)$$

where $\theta_3 = \tan^{-1}[\frac{\rho_1 \sin(\theta_0 - \theta_1) + \rho_2 \sin(\theta_2 - \theta_0)}{\rho_1 \cos(\theta_0 - \theta_1) + \rho_2 \cos(\theta_2 - \theta_0)}]$.

If ω_0 is located right at or near the Bragg frequency of the uniform FBG and $\omega_m << \omega_0$, we have the approximation $|\rho_1| \approx |\rho_2| \approx |\rho_0|$. Then Eq. (5.18) can be simplified as

$$y(t) = \frac{1}{2} m_a E_0^2 |\rho_0|^2 \cos(\frac{\theta_2 + \theta_1}{2} - \theta_0) \cos(\omega_m t + \frac{\theta_2 - \theta_1}{2}). \quad (5.19)$$

Substituting Eq. (5.15) into Eq. (5.19), we get

$$y(t) = \frac{1}{2} m_a E_0^2 |\rho_0|^2 \cos(\frac{1}{2} D\omega_m^2 + \frac{5}{8} \ddot{D}\omega_m^4) \cos[\omega_m t + z\dot{\beta}(\omega_0)\omega_m + \frac{1}{3}\dot{D}\omega_m^3], \quad (5.20)$$

where $z\dot{\beta}(\omega_0)$ is a constant time delay determined by the FBG length, and $z\dot{\beta}(\omega_0)\omega_m$ is the basic phase shift with respect to the modulating frequency ω_m. It is easily seen from Eq. (5.20) that the FBG induced dispersion introduces undesired phase shift $\frac{\dot{D}}{3}\omega_m^3$ and amplitude fluctuation $\cos(\frac{1}{2} D\omega_m^2 + \frac{5}{8} \ddot{D}\omega_m^4)$.

5.4 Evaluation of FBG-induced dispersion effects

To evaluate the dispersion effects on the all-optical microwave filters, the reflection spectra, group delays, first, second and third order dispersions are calculated for four different uniform FBGs. Fig 5.1 shows the simulated results for two FBGs with identical length, $L = 1\ mm$, but different peak

reflectivities. Fig 5.2 shows the simulated results for two FBGs with same peak reflectivity but different lengths; 4 *mm* and 10 *mm*.

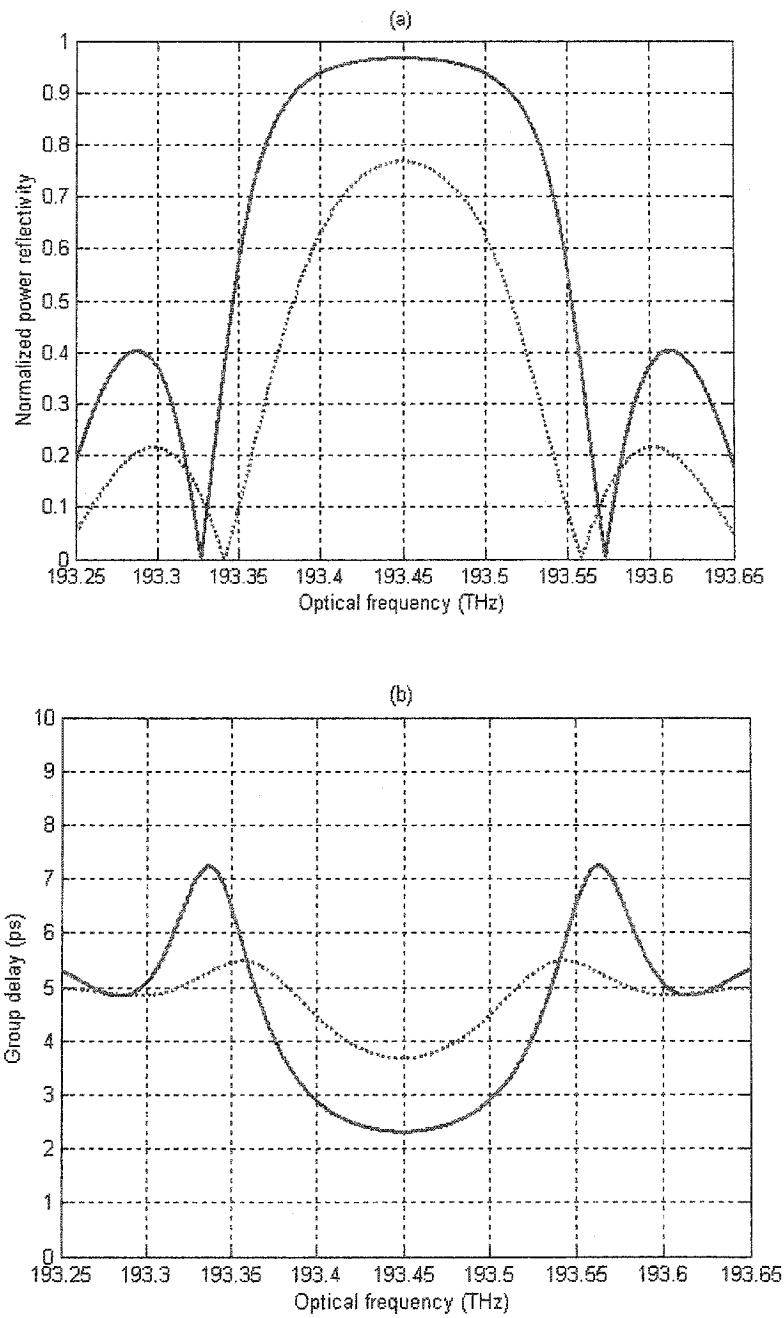

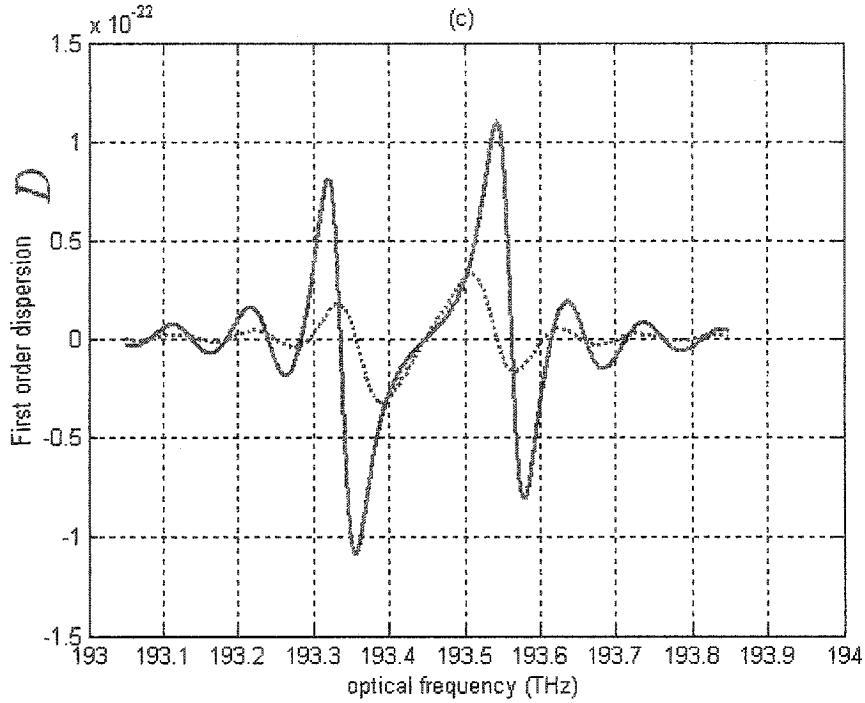
(c)
x 10^-22
1.5
1
0.5
0
-0.5
-1
-1.5
First order dispersion D
193
193.1
193.2
193.3
193.4
193.5
193.6
193.7
193.8
193.9
194
optical frequency (THz)

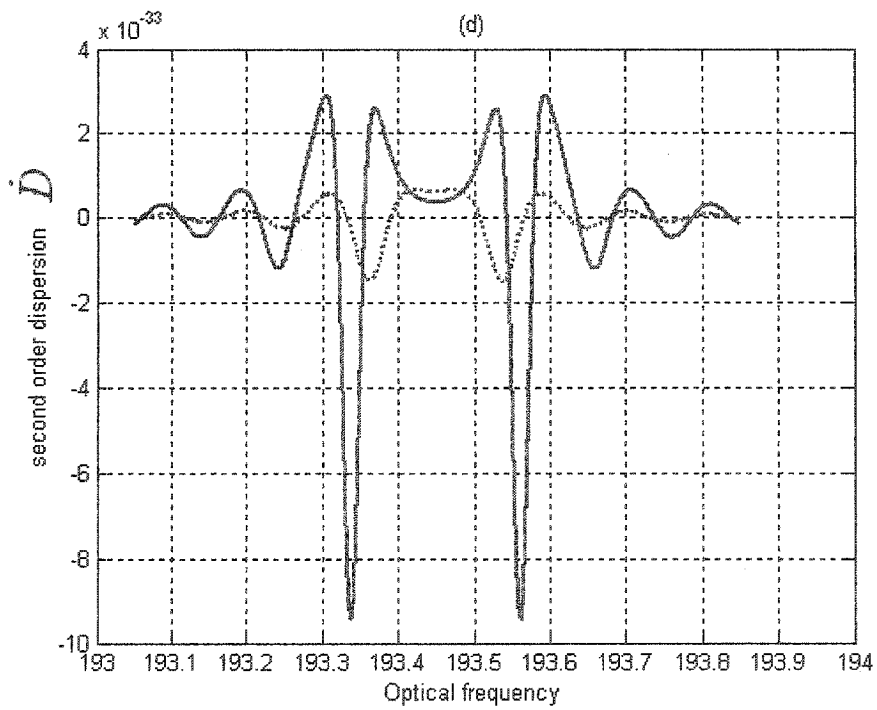
(d)
x 10^-33
4
2
0
-2
-4
-6
-8
-10
second order dispersion D'
193
193.1
193.2
193.3
193.4
193.5
193.6
193.7
193.8
193.9
194
Optical frequency

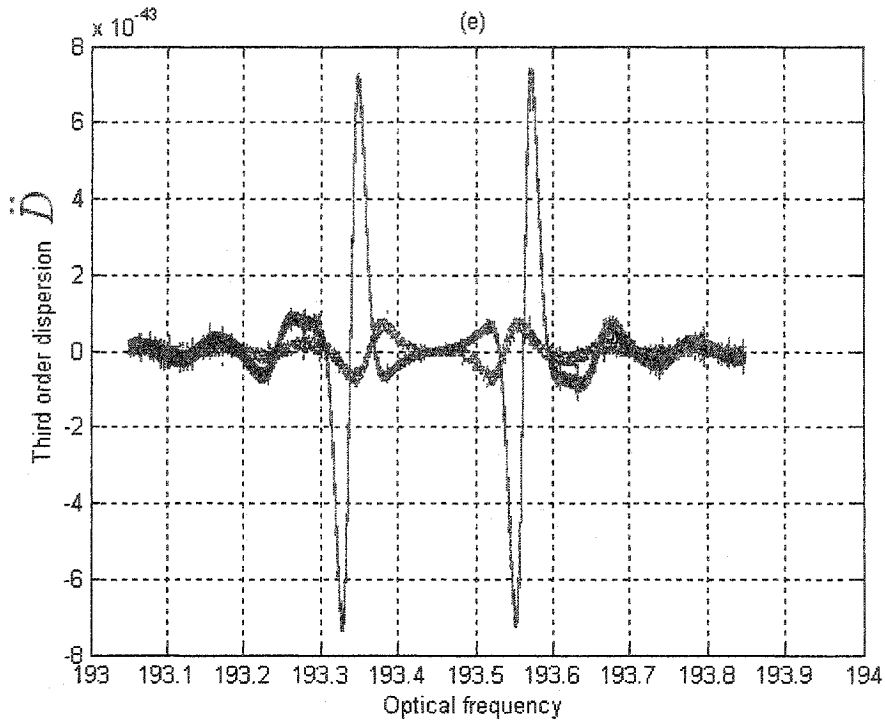

Fig 5.1 Simulated results for two FBGs with identical length $L = 1\ mm$, but different peak reflectivities. Solid line: $\overline{\delta}_{neff} = 1 \times 10^{-3}$; dotted line: $\overline{\delta}_{neff} = 5 \times 10^{-4}$.

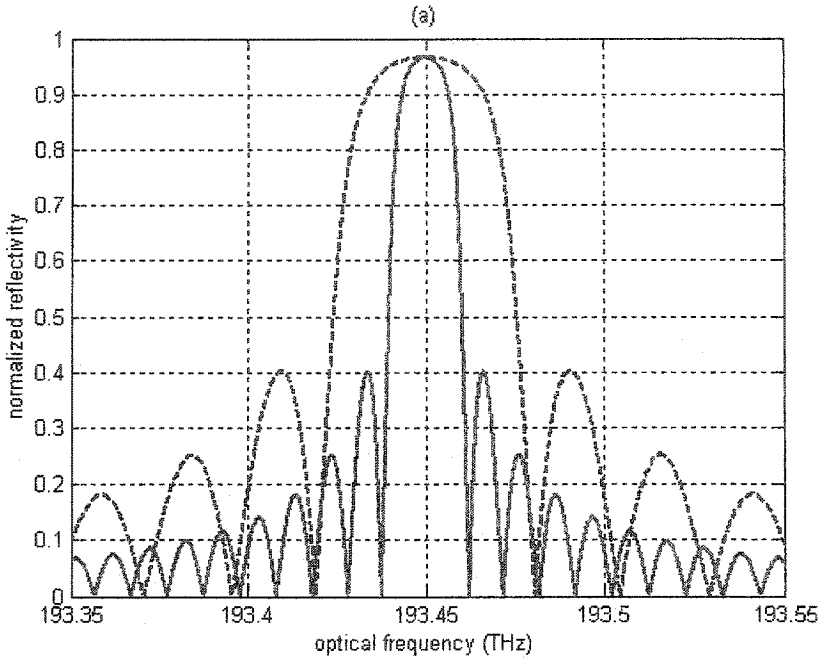
(a)
normalized reflectivity
optical frequency (THz)
0
0.1
0.2
0.3
0.4
0.5
0.6
0.7
0.8
0.9
1
193.35
193.4
193.45
193.5
193.55

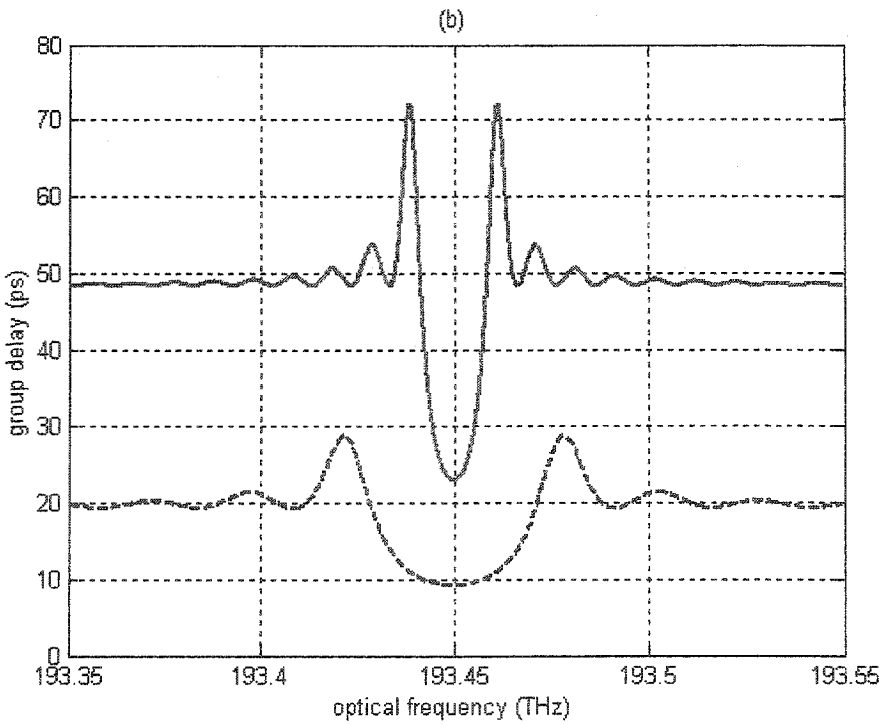
(b)
group delay (ps)
optical frequency (THz)
0
10
20
30
40
50
60
70
80
193.35
193.4
193.45
193.5
193.55

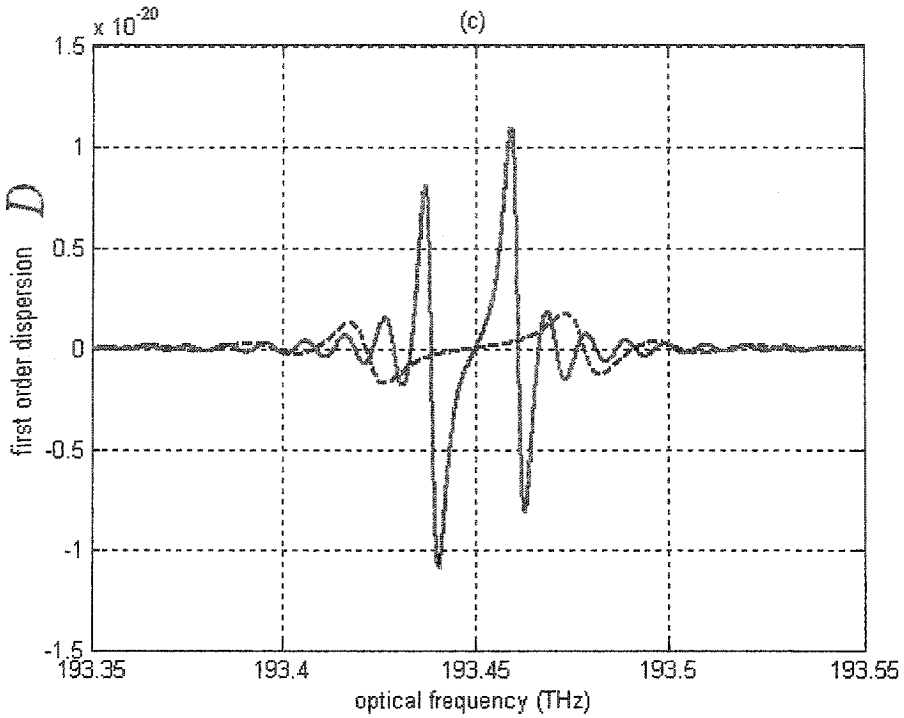
(c)
x 10^-20
1.5
1
0.5
0
-0.5
-1
-1.5
first order dispersion D
193.35
193.4
193.45
193.5
193.55
optical frequency (THz)

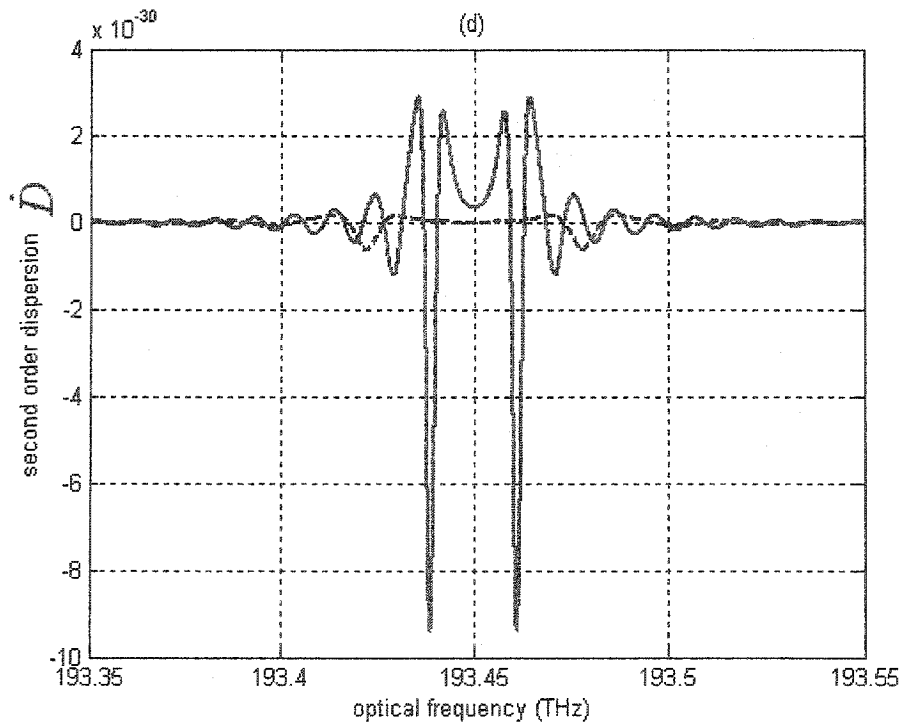
(d)
x 10^-30
4
2
0
-2
-4
-6
-8
-10
second order dispersion D̂
193.35
193.4
193.45
193.5
193.55
optical frequency (THz)

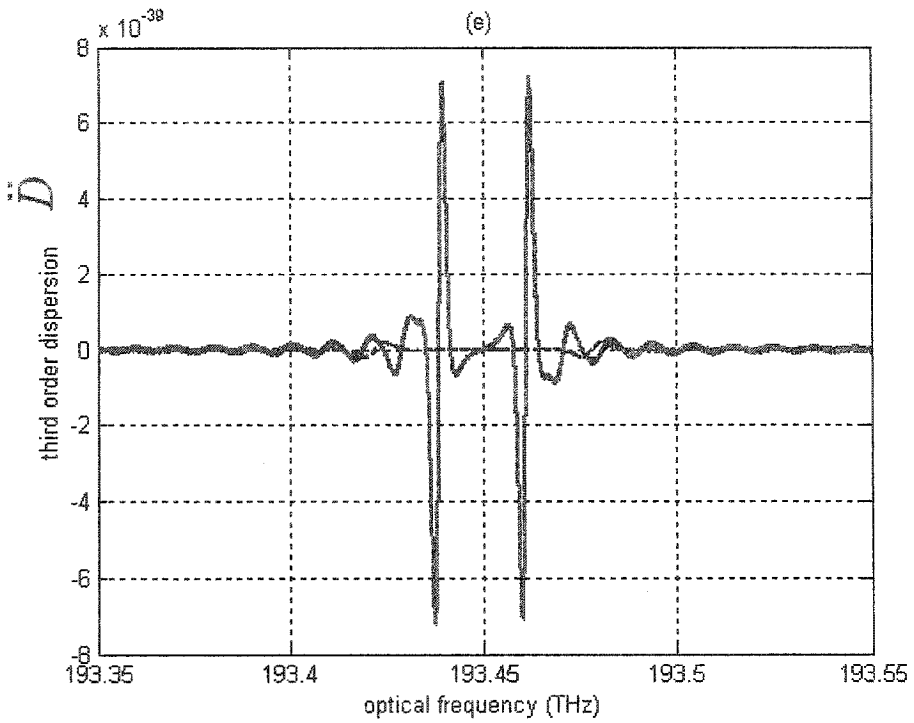

Fig 5.2 Simulated results for two FBGs with same peak reflectivity but different lengths. Solid line: $L = 10\,mm$, $\overline{\delta}_{neff} = 1\times10^{-4}$; dotted line: $L = 4\,mm$, $\overline{\delta}_{neff} = 2.5\times10^{-4}$.

By studying these plots, we have the following conclusion:

First, the null-to-null bandwidth is inversely proportional to the grating length for weak gratings and when the grating gets stronger, the reflection bandwidth is proportional to the index variation, which can be easily seen from Fig 5.1(a) and Fig 5.2 (a).

Second, most power is reflected within the FWHM bandwidth.

Third, group delays and dispersions are small within the FWHM frequency range, whereas they fluctuate significant near the band edge and decrease rapidly outside the main lobe of the reflection band.

Before we analyze the dispersion effects on the FBG-based microwave filters, we start with a simple example using the equations we obtained in Section 5.3: the dispersion effects on the FBG-based true time-delay beamforming networks for phased array antennas. The reason we think this is a simple example is that in the FBG-based true time-delay beamforming networks, the light source has single frequency. The analysis is a direct application of the equations derived in Section 5.3, but the results can be extended to the systems using a broadband light source, such as the FBG-based microwave filters discussed in this thesis, where the light source can be considered as a combination of many single-frequency light sources.

Eq. (5.20) is obtained assuming that the light source has a single frequency; we will apply it to analyze the dispersion effects on FBG-based true-time delay phased array beamforming networks.

In true time-delay beamforming networks, a single frequency source is usually used. Fig 5.3 shows an N-channel uniform FBG-based true time-delay beamforming network. It consists of a wavelength tunable laser, a high speed EOM and N FBG arrays serving as an FBG prism. The tunable laser source is externally modulated by an RF signal using the EOM. The modulated optical signal is then fed to the N-channel FBG arrays by a 1: N optical splitter and N three-port circulators. Each FBG array has M uniform FBGs; each FBG reflects light at a specific wavelength λ_j ($j = 1, 2, ..., M$). The spacing between adjacent FBGs increases linearly from channel 1 to channel N. The N-channel time-delayed signals are sent to N photodetectors to convert the time-delayed optical signals to RF signals. The RF signals are amplified by pre-amplifiers and power amplifiers and then fed to N phased antenna array elements. A radiation pattern is generated at the far field [93-94] [96]. The direction of the radiation pattern is steered by tuning the wavelength of the tunable laser source.

The far field beam pattern formed at λ_j can be expressed as

$$F_j(\alpha) = \sum_{i=1}^{N} A_{ij} e^{-j[\varphi_{ij} + (i-1)\frac{2\pi\omega_m}{c} d \cdot \sin\alpha]}, \tag{5.21}$$

where A_{ij} is the amplitude of the RF signal fed to the i-th (i = 1, 2, ..., N) antenna when the beam pointing angle are supposed to steer at α_j, φ_{ij} represents the phase delay introduced by the FBG prism, ω_m is the frequency of the RF signal, c is the velocity of light in free space, d is the spacing between the adjacent antenna elements.

As can be seen in our discussion in Section 5.3, the dispersion caused by the FBGs not only introduces undesired phase shift, but also leads to amplitude degradation if DSB modulation scheme is employed. To achieve wideband operation, the first and higher order dispersion should be suppressed to make phase shift term $\dot{D}\omega_m^3/3$ small and amplitude fluctuation term $\cos(D\omega_m^2/2 + 5\ddot{D}\omega_m^4/8)$ near unity. Based on Fig 5.1 and Fig 5.2, if we choose FBGs with short length and relatively small reflectivity, the dispersion effects can be significant reduced. Theoretically, if the optical carrier frequency ω_0 is equal to the Bragg frequency, D and $\ddot{D}$ are equal to zero and no limitation on the highest operating frequency of the beamforming network.

True time delay beamforming can also be realized using a chirped grating [99-100]. In a chirped grating-based network, the linear chirped FBG gives a linear group delay within a wide reflection bandwidth, thanks to the change of the

Bragg wavelength with the position along the grating. This implies that the first order dispersion D of linear chirped FBG is a non-zero constant and higher-order dispersions are zeros. In real applications, to achieve wide beam steering range within limited available wavelength band of the tunable laser, large D is preferred, which will significantly limit the highest operating frequency and the bandwidth of the chirped grating-based beamforming networks [86] [90].

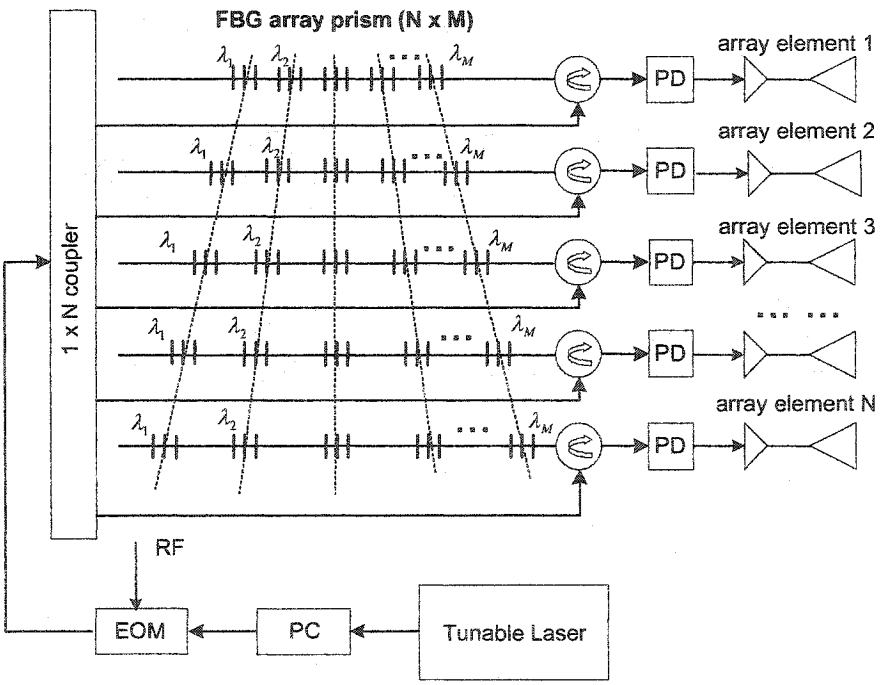

Fig 5.3 Uniform FBG-based true time-delay beamforming network.

To further reduce or eliminate the dispersion effects, single side band (SSB) modulation would be employed, which can be implemented by either using a

very narrow band FBG to remove one side band directly or using two phase modulators by mixing of the two unbalanced phase-modulated light beams driven by a pair of microwave signals with a phase shift of $\pi/2$ [87] [91]. When the SSB modulation technique is applied, the amplitude of the recovered RF signal is independent of the phase shift because the amplitudes and phases of the modulated signal do not include any beating between two frequency terms, as can be seen in Eq. (5.6). In this case, there is not any cancellation of the modulated signal. However, the dispersion-induced phase shift still exists, and is expressed as

$$\theta_2 - \theta_0 = z\dot{\beta}(\omega_0)\omega_m + \frac{D}{2}\omega_m^2 + \frac{\dot{D}}{3}\omega_m{}^3 + \frac{5}{8}\cdot\ddot{D}\omega_m{}^4 + \cdots. \tag{5.22}$$

Although the FBG synthesis parameters can be carefully chosen to minimize the dispersion-induced phase shift, the phase shift cannot be completely eliminated, which will limits the highest operating frequency for true time-delay based applications.

It is different from the true time delay beamforming networks where a single frequency light source is used, the all-optical microwave filters discussed in

this thesis are based on a broadband light source. Let us rewrite Eq. (5.20) by replacing the single frequency carrier by a bunch of frequencies,

$$y(t) = \sum_k \{\frac{1}{2} m_{a,k} E_k^2 |\rho_k|^2 \cos(\frac{1}{2} D_k \omega_m^2 + \frac{5}{8} \ddot{D}_k \omega_m^4) \cdot \cos[\omega_m t + z\dot{\beta}(\omega_k)\omega_m + \frac{1}{3} \dot{D}_k \omega_m^3]\}, \quad (5.23)$$

where ρ_k denotes the complex amplitude reflectivity at ω_k; $D_k, \dot{D}_k, \ddot{D}_k$ are respectively the 1st, 2nd and 3rd order dispersions at ω_k. We again assume $\omega_m << \omega_k$. Based on Eq. (5.23), the recovered RF signal reflected by the *m*-th FBG in the FBG array is composed of a bunch of electrical signals with identical frequency ω_m, but different amplitudes and phases. We can see that the amplitude and phase shift are the functions of the modulating frequency and the synthesis parameters.

Fortunately, when the modulating frequency is not very high, we can get good approximation that the filter coefficients are constant for different modulating frequencies and the dispersion induced phase shifts can be neglected. For example, from Fig 4.8 (c), (d) and (e), considering the FBG with length of 1 mm and $\bar{\delta}_{neff} = 5 \times 10^{-4}$, its group delay, first, second and third order dispersions at the edge of its 3-dB bandwidth are respectively at the level of

$\tau = 5ps$, $D = 1\times10^{-22} s/(Hz\cdot 2\pi)$, $\dot{D} = 1\times10^{-33} s/(Hz\cdot 2\pi)^2$ and $\ddot{D} = 1\times10^{-43} s/(Hz\cdot 2\pi)^3$. Substituting these numbers into Eq. (5.23), and take $\omega_m = 10GHz\cdot 2\pi$, we get $\cos(D\omega_m^2/2 + 5\ddot{D}\omega_m^4/8) = 0.9994$, the power degradation, and $\dot{D}\omega_m^3/3 = 0.6\times10^{-3}\pi$, the undesired phase shift for the *i*-th frequency component. The 3-dB and the first-null modulating frequencies can be calculated by letting $\cos(D\omega_m^2/2 + 5\ddot{D}\omega_m^4/8) = 0.5$ and $\cos(D\omega_m^2/2 + 5\ddot{D}\omega_m^4/8) = 0$, which are respectively 35.8 GHz and 92.8 GHz in this example. For the carrier frequency components which are closer to the FBG center frequency, the corresponding recovered RF signals degrade much slower than those near the band edge. At the same time, they contribute more reflected power to the output because the reflectivity at or near the Bragg wavelength is much higher than those near the reflection band edge. These results indicate that when the modulating frequency is at 10 GHz or lower, the dispersion effects can be ignored.

If the FBGs with longer length, such as those described in Fig 5.2, are used to implement the filter, and the effective coefficients are still calculated using Eq. (4.4), more errors in the effective coefficients will be presented because longer FBGs introduce more dispersion effects than shorter FBGs, such as those

described in Fig 5.1. This result shows that FBGs with shorter length and weaker reflectivity induce much less dispersion.

5.5 Summary

In this chapter we have studied the dispersion effects on the FBG-based all-optical microwave filters. We found that the dispersion effects could result in the amplitude fluctuation and undesired phase shift for the time delayed RF signals detected at the photodetector, which would limit the highest operating frequency of the all-optical microwave filters. We also found that the effective coefficients obtained using the genetic algorithm would be changed due to the dispersion effects, which would degrade the performance of the all-optical microwave filters. To reduce the dispersion effects, we proposed to use short and weak FBGs, but this would cause implementation errors. A second method that could be used to reduce or almost eliminate the dispersion effects was to use single side band modulation, at the cost of a more complicated system.

Chapter 6

CONCLUSIONS AND FUTURE WORK

6.1 Conclusions

The three objectives of this work were (1) to synthesize FBG-based all-optical microwave filters using genetic algorithms, (2) to realize of the filters with the designs using genetic algorithms, and (3) to analyze the dispersion effects on the FBG-based all-optical microwave filters. All the three objectives have been achieved.

In Chapter 2, the theory model of uniform FBG-based all-optical microwave filter was presented. The key components including the electro-optic modulators, photo-detectors, FBGs were introduced in this Chapter.

In Chapter 3, the synthesis of FBG-based all-optical microwave filters using the genetic algorithms was proposed. In the proposed algorithm, all-optical microwave filters employing fiber Bragg gratings as tapping and weighting elements were considered. The coefficients and the tapping intervals of the

microwave filters were optimized by the genetic algorithm. Algorithms for fixed and variable tapping intervals were developed and two design examples were presented and discussed.

In Chapter 4, we discussed the implementation of the all-optical microwave filters. Two FBG arrays were fabricated based on the design using the genetic algorithms. All-optical microwave filters based on the two FBG arrays were constructed and characterized. To achieve the optimal filter response, the filter coefficients have to be calibrated. We showed by considering both the power spectrum of the optical source and the power reflectivities of the FBGs, filter response identical to the design objective was achieved.

Dispersion effects on the performance of uniform FBG-based all-optical microwave filter were discussed in Chapter 5. We found the dispersion effects would lead to amplitude fluctuation and unwanted phase, which would reduce the performance of the all-optical microwave filters. We showed that the dispersion effects could be reduced by using short and weak fiber Bragg gratings, but adding to implementation errors because of the difficult in producing accurate weak gratings. The dispersion effects could be reduced or almost eliminated if single-side band modulation scheme was used.

6.2 Future work

We should note that in the design of the all-optical microwave filters, the coefficients are constraint with positive values due to the incoherent interference, which prevents the inclusion of negative coefficients. By applying the time-delayed light signals to two photodetectors with differential detection, all-optical microwave filters with negative coefficients can be implemented in the optical domain [19] [64-65]. Other techniques such as using cross gain modulation (XGM) of a semiconductor optical amplifier (SOA) can also be used to implement all-optical microwave filters with negative coefficients [101-106]. These techniques open the way to implement all types of all-optical microwave filters, such as band-pass filters and high-pass filters.

In this research project, the filters are synthesized based on an array of FBGs with a broadband light source. In communications and radio-over-filter systems, the light sources are usually semiconductor lasers with narrow bandwidth and high coherence. All-optical microwave filters that can be incorporated into these systems for all-optical microwave filtering would be investigated.

In this research, the attention was paid to the amplitude of the transfer functions of the all-optical microwave filters, and no phase information was used in the filter design. For many applications, the phase information is important and should be considered in the all-optical microwave filter design. Further research would be carried out to design and implement all-optical microwave filters with both amplitude and phase information taking into account.

BIBLIOGRAPHY

[1]. J. L. Horner, *Optical Signal Processing*. Academic Press, 1987.

[2]. P. M. Grant and R. S. Withers, "Recent advances in analog signal processing," IEEE Trans. Aerospace and Electron. System, vol. 26, pp. 818-849, Sept. 1990.

[3]. Wang. W. C, "Special issue on SAW convolvers and correlators," IEEE Trans. Sonics and Ultrasonics, SU-32, 5, Sept. 1985.

[4]. M. F. Lewis, C. L. West, J. M. Deacon, and R. F. Humphries, "Recent developments in SAW devices," IEE Proceedings, 131, pt. A, no. 4, pp. 186-215, Jun. 1984.

[5]. R. S. Withers, A. C. Anderson, J. B. Green, and S. A. Reible, "Superconductive delay-line technology and applications," IEEE Trans. Magnetics, MAG-21, no. 2, pp. 186-192, Mar. 1985.

[6]. A. Oppenheim, R. Schaffer and J. R. Buck, *Discrete-Time Signal Processing*. Upper Saddle River, NJ: Prentice-Hall, 1998.

[7]. JOHN g. Proakis, and Dimitris G. Manolakis, *Digital signal processing: principles, algorithms and applications*. Upper Saddle River, NJ: Prentice-Hall, 1996.

[8]. K. P. Jackson, S. A. Newton, B. Moslehi, M. Tur, C. C. Cutler, J.W. Goodman and H. J. Shaw, "Optical fiber delay line signal processing,"

IEEE Trans. Microwave Theory Technol., vol. MTT-33, pp. 193-209, Mar. 1985.

[9]. K. Wilner, A. P. Van den Heuvel, "Fiber-optic delay lines for microwave signal processing," Proc. IEEE, vol. 64, pp. 805-807, 1976.

[10].M. A. Muriel, J. Azana, and A. Carballar, "Real-time Fourier transformer based on fiber gratings," Optics Lett., vol. 24, no. 1, pp. 1-3, Jan. 1999.

[11].J. Azana, L. R. Chen, M. A. Muriel and P. W. E. Smith, "Experimental demonstration of real-time Fourier transformation using linearly chirped fiber Bragg gratings," Electron. Lett., vol. 35, no. 25, pp. 2223-2224, Dec. 1999.

[12].M. C. Cardakli, and A. E. Willner, "Synchronization of a network element for optical packet switching using optical correlators and wavelength shifting," IEEE Photon. Technol. Lett., vol. 14, no.9, pp. 1375 -1377, Sept. 2002.

[13].H. J. S. Dorren, M. T. Hill, Y. Liu, N. Calabretta, A. Srivatsa, F. M. Huijiskens, H. de Waardt, and G. D. Khoe, "Optical packet switching and buffering by using all-optical signal processing methods," J. Lightwave Technol., vol. 21, no. 1, pp. 2-12, Jan. 2003.

[14].S. Gweon, C. E. Lee, and H. F. Taylor, "Wide-band fiber optic signal processor," IEEE Photon. Technol. Lett., vol. 1, pp. 467, Dec. 1989.

[15].S. Gweon, C. E. Lee, and H. F. Taylor, "Programmable fiber optic signal processor," IEEE Photon. Technol. Lett., vol. 2, pp. 382-384, May. 1990.

[16].K. Sasayama, M. Okuno, and K. Habara, "Coherent optical transversal filter using silica-based waveguides for high-speed signal processing," J. Lightwave Technol., vol. 9, no. 10, pp. 1225-11230, Oct. 1991.

[17].S. T. Johns, D. A. Norton, C.W. Keefer, R. Erdmann, R.A. Soref, "Variable time delay of microwave signals using high Dispersion fiber", Electron. Lett., vol. 29, pp. 555-556, Mar. 1993.

[18].J. Capmany and J. Cascon, "Direct Form I fiber-optic discrete-time signal processors using optical amplifiers and embedded Mach-Zehnder structures," IEEE Photon. Technol. Lett., vol. 5, no. 7, pp. 842-844, Jul. 1993.

[19].I. Andonovic, L. Tancevski, M. Shabeer, and L. Bazgaloski, "Incoherent all-optical code recognition with balanced detection," J. Lightwave Technol., vol. 12, no. 6, pp. 1073-1080, Jun. 1994.

[20].D. Norton, S. Johns, C. Keefer and R. Soref, "Tunable microwave filtering using high dispersion fiber time delays," IEEE Photon. Technol. Lett., vol. 6, pp. 831-832, Jul. 1994.

[21].J. Capmany and J. Cascon, "Discrete time fiber-optic signal processors using optical amplifiers," J. Lightwave Technol., vol. 12, no. 1, pp. 106-117, Jan. 1994.

[22].S. Tedjini, A. Ho-Quoc and D. Khalil, "All-optical networks as microwave and millimeter wave circuits," IEEE Trans. Microwave Theory Technol., vol. 43, pp. 2428-2434, Sept. 1995.

[23].S. Sampson, R. Griffin and D. Jackson, "Photonic CDMA by coherent matched filtering using time-address coding in optical ladder networks," J. Lightwave Technol., pp. 2001-2010, Nov. 1994.

[24].D. B. Hunter, R. Minasian and P. A. Krug, "Tunable optical transversal filter based on chirped gratings," Electron. Lett., vol. 31, no. 25, pp. 2207-2210, Dec. 1995.

[25].M. Frankel and R. Esman, "Fiber-optic tunable microwave transversal filter," IEEE Photon. Technol. Lett., vol. 7, pp. 191-193, Feb. 1995.

[26].D. B. Hunter and R. Minasian, "Reflectivity tapped fiber optic transversal filter using in-fiber Bragg gratings," Electron. Lett., vol. 31, pp. 1010-1012, Jun. 1995.

[27].J. D. Shin, M. Y. Jeon and C. S. Kang, "Fiber-optic matched filters with metals films deposited on fiber delay line ends for optical packet address detection," IEEE Photon. Technol. Lett., vol. 8, pp. 941-943, Jul. 1996.

[28].A. P. Foord, P. A. Davies, and P. A. Greenhalgh, "Synthesis of microwave and millimeter-wave filters using optical spectrum-slicing", Electron. Lett., vol. 32, no. 4, pp. 390-391, Feb. 1996.

[29].F. Coppinger, S. Yegnanarayanan, P. D. Trinh, and B. Jalali, "Continuously tunable photonic radio-frequency notch filter," IEEE Photon. Technol. Lett., vol. 9, no. 3, pp. 339-341, Mar. 1997.

[30].D. B. Hunter and R. Minasian, "Microwave optical filters using in-fiber Bragg grating arrays," IEEE Microwave and Guided Wave Lett., vol. 6, pp. 103-105, Feb. 1996.

[31].D. B. Hunter and R. Minasian, "Photonic signal processing of microwave signals using an active-fiber Bragg-grating-pair structure," IEEE Trans. Microwave Theory and Technol., vol. MTT-45, pp. 1463-1466, Aug. 1997.

[32].J. Marti, F. Ramos and R. I. Laming, "Photonic microwave filter employing multimode optical sources and wideband chirped fiber gratings," Electron. Lett., vol. 34, no. 18, pp. 1760-1761, Sept. 1998.

[33].F. Coppinger, C. K. Madsen, and B. Jalali, "Photonic microwave filtering using coherently coupled integrated ring resonators", Microwave and Optical Technol. Lett., vol. 21, no. 2, pp. 90-93, Apr. 1999.

[34].J. Capmany, D. Pastor and B. Ortega, "Efficient sidelobe suppression by source power apodization in fiber optic microwave filters composed of linearly chirped fiber grating by laser array," Electron. Lett., vol. 35, no. 8, pp. 640-642, Apr. 1999.

[35].J. Capmany, D. Pastor and B. Ortega, "New and flexible fiber-optic delay-line filters using chirped Bragg gratings and laser arrays," IEEE Trans. Microwave Theory and Technol., vol. 47, no. 7, pp. 1321-1326, Jul. 1999.

[36].N. You and R. A. Minasian, "A novel high-Q optical microwave processor using hybrid delay-line filters," IEEE Trans. Microwave Theory and Technol., vol. 47,no. 7, pp. 1304-1308, Jul. 1999

[37].D. B. Hunter and R. A. Minasian, "Tunable microwave fiber-optic bandpass filters," IEEE Photon. Technol. Lett., vol. 11, no. 7, pp. 874-876, Jul. 1999.

[38].J. Marti, V. Polo, F. Ramos and D. Moodie, "Photonics tunable microwave filters employing electro-absorption modulators and wideband chirped fiber gratings," Electron. Lett., vol. 35, no. 4, pp. 305-306, Feb. 1999.

[39].D. Pastor, J. Capmany and B. Ortega, "Experimental demonstration of parallel fiber-optic-based RF filtering using WDM techniques," IEEE Photon. Technol. Lett., vol. 12, no. 1, pp. 77-78, Jan. 2000.

[40].B. Ortega, J. L. Cruz, J. Capmany, M. V. Andres and D. Pastor, "Analysis of a microwave time delay line based on a perturbed uniform fiber Bragg grating operating at constant wavelength," J. Lightwave Technol., vol. 18, no. 3, pp. 430-436, Mar. 2000.

[41].G. Yu, W. Zhang, and J. A. R. Williams, "High-performance microwave transversal filter using fiber Bragg grating arrays," IEEE Photon. Technol. Lett., vol. 12, no. 9, pp. 1183-1185, Sept. 2000.

[42].D. Pastor, J. Capmany, and B. Ortega, "Broad-band tunable microwave transversal notch filter based on tunable uniform fiber Bragg gratings as slicing filters," IEEE Photon. Technol. Lett., vol. 13, no. 7, pp. 726-728, Jul. 2001.

[43].R. A. Minasian, K. E. Alameh, and Erwin H. W. Chan, "Photonics-based interference mitigation filters," IEEE Trans. Microwave Theory and Technol., vol. 49, no. 10, pp. 1894-1899, Oct. 2001.

[44].N. You and R. A. Minasian, "A novel tunable microwave optical notch filter," IEEE Trans. Microwave Theory and Technol., vol. 49, no. 10, pp. 2002-2005, Oct. 2001.

[45].H. Sotobayashi and Ken-ichi Kitayama, "Transfer response measurements of a programmable bipolar optical transversal filter by using the ASE noise of an EDFA," IEEE Photon. Technol. Lett., vol. 11, no. 7, pp. 871-873, Nov. 2001.

[46].S. Sales, J. Capmany, J. Marti and D. Pastor, "Novel and significant results on the non-recirculating delay line with a fiber loop," IEEE Photon. Technol. Lett., vol. 7, no. 12, pp. 1439-1440, Dec. 2001.

[47]. W. Zhang, J. A. R. Williams and I. Bennion, "Optical fiber recirculating delay line incorporating a fiber grating array," IEEE Microwave and Wireless Components Lett., vol. 11, no. 5, pp. 217-219, May. 2001.

[48]. W. Zhang, J. A. R. Williams, and I. Bennion, "Polarization synthesized optical transversal filter employing high birefringence fiber gratings," IEEE Photon. Technol. Lett., vol. 13, no. 5, pp. 523-525, May. 2001.

[49]. D. Pastor, J. Capmany, S. Sales, P. Munoz and B. Ortega, "Reconfigurable fiber-optic-based RF filters using current injection in multimode lasers," IEEE Photon. Technol. Lett., vol. 13, no. 11, Nov. 2001.

[50]. B. Vidal, "Optical delay line based on arrayed waveguide gratings' spectral periodicity and dispersive media for antenna beamforming applications," IEEE Journal of Quantum Electronics, vol. 8, no. 6, Nov/Dec. 2002.

[51]. K. H. Lee, W. Y. Choi, S. Choi and K. Oh, "A novel tunable fiber-optic microwave filter using multimode DCF," IEEE Photon. Technol. Lett., vol. 15, no. 7, Jul. 2003.

[52]. V. Polo, B. Vidal, J. L. Corral, and J. Marti, "Novel tunable photonics microwave filter based on laser arrays and NxN AWG-based delay lines," IEEE Photon. Technol. Lett., vol. 15, no. 4, pp. 584-586, Apr. 2003.

[53].F. T. S. Yu, S. Jutamulia and S. Yin, *Introduction to information optics.* Academic Press, San Diego, 2001.

[54].G. P. Agrawal, *Fiber-optic communication systems.* John Wiley & Sons, NY, 2002.

[55].M. M. Ohn, A. T. Alavie, R. Maaskant, M. G. Xu, F. Bilodeau and K. O. Hill, "Dispersion variable fiber Bragg grating using a piezoelectric stack," Electron. Lett., vol. 32, no. 21, pp. 2000-2001, 10th Oct. 1996.

[56].T. Imai, T. Koumukai and M. Nakazawa, "Dispersion tuning of a linearly chirped fiber Bragg grating without a center wavelength shift by applying a strain gradient," IEEE Photon. Technol. Lett., vol. 10, no. 6, pp. 845-847, Jun. 1998.

[57].Y. Liu, J. P. Yao, X. Dong and J. Yang, "Tunable chirping of a fiber Bragg grating without center wavelength shift using simply supported beam," SPIE Journal - Optical Engineering vol. 41, pp. 740 - 741, Apr. 2002.

[58].J. Mora, B. Ortega, M. V. Andres, J. Capmany, D. Pastor, J. L. Cruz and S. Sales, "Tunable chirped fiber Bragg grating device controlled by variable magnetic fields," Electron. Lett., vol. 38, no. 3, pp. 118-119, 31st Jan. 2002.

[59].Turan Erdogan, "Fiber grating spectra," Invited paper of J. Lightwave Technol., vol. 15, no. 8, pp. 1277-1294, Aug. 1997.

[60].Amnon Yariv, "Coupled-mode theory for guided-wave optics," IEEE Journal of Quantum Electronics, vol. QE-9, no. 9, pp. 919-933, Sept. 1973.

[61].A. Carballar and M. A. Muriel, "Phase reconstruction from reflectivity in fiber Bragg gratings," J. Lightwave Technol., vol. 15, no. 8, pp. 1314-1322, Aug. 1997.

[62].C. K. Madsen, and J. H. Zhao, *Optical filter design and analysis: a signal processing approach.* John Wiley & Sons, NY, 1999.

[63].E. C. Heyde and R. A. Minasian, "A solution to the synthesis problem of recirculating optical delay line filter," IEEE Photon. Technol. Lett., vol. 6, pp. 833-835, Jul. 1994.

[64].J. Capmany, J. Cascon, J. L. Martin, S. Sales, D. Pastor, J. Marti, "Synthesis of fiber-optic delay line filters," J. Lightwave Technol., vol. 13, pp. 2003-2012, Oct. 1995.

[65].S. Sales, J. Capmany, J. Martin, D. Pastor., "Experimental demonstration of fiber-optic delay filters with negative coefficients," Electron. Lett., vol. 31, no. 13, pp. 1095-1096, Jun. 1995.

[66].J. Capmany, J. Martin, "Solutions to the synthesis problem of optical delay line filters," Opt. Lett., vol. 20, no. 23, pp. 2438-2440, Dec. 1995.

[67].T. A. Cusick, S. Iezekiel, R.E Miles, S. Sales, J. Capmany, "Synthesis of all-optical microwave filters using Mach-Zehnder lattices," IEEE Trans. Microwave Theory and Technol., vol. 45, pp. 1458-1462, Aug. 1997.

[68].T. A. Cusick, S. Iezekiel, R. E. Miles "All-optical microwave filter design employing a genetic algorithm," IEEE Photon. Technol. Lett., vol. 10, no. 8, pp.1156-1158, Aug. 1998.

[69].L. Benvenuti and L. Farina, "The design of fiber-optic filters," J. Lightwave Technol., vol. 19, no. 9, pp. 1366-1375, Sept. 2001.

[70].K. S. Tang, K. F. Man, S. Kwong and Q. He, "Genetic algorithms and their applications," IEEE signal processing magazine, pp. 22-37, Nov. 1996.

[71].David. A. Coley, *An introduction to Genetic Algorithms for Scientists and Engineers*. ISBN 981-02-3602-6, 1999.

[72].Zbigniew Michalewicz, *Genetic Algorithms + Data Structures=Evolution Programs*. Springer-Verlag, NY, 1996.

[73].D. Suckley, "Genetic algorithm in the design of FIR filters," IEE Proceedings-G, vol. 138, no.2, pp. 234-238, Apr. 1991.

[74].Q. C. Meng, T. J. Feng, Z. Chen, C. J. Zhou, and J. H. Bo, "Genetic algorithms encoding study and a sufficient convergence condition of Gas," Systems, Man, and Cybernetics, 1999. IEEE SMC '99 Conference

Proceedings. 1999 IEEE International Conference on, vol. 1, pp. 649 - 652, Oct. 1999.

[75].T. Arslan, and D. H. Horrocks, "The design of analogue and digital filters using genetic algorithms," IEE 15th SARAGA Colloquium on, pp. 2/1 - 2/5, Nov. 1995.

[76].S. P. Harris and E. C. Ifeachor, "Automatic design of frequency sampling filters by hybrid genetic algorithm techniques," IEEE Trans. Signal Processing, vol. 46, no. 12, Dec. 1998.

[77].A. Lee, M. Ahmadi, G. A. Jullien, W. C. Miller, and R. S. Lashkari, "Digital filter design using genetic algorithm," Advances in Digital Filtering and Signal Processing, 1998 IEEE Symposium on, pp. 34 -38, Jun. 1998.

[78].A. Lee, M. Ahmadi, G. A. Jullien, W. C. Miller, and R. S. Lashkari, "Design of 1-D FIR filters with genetic algorithms," 5th International Symposium on Signal Processing and its Applications, pp. 955-958, ISSPA'99, Australia, Aug. 1999.

[79].A. Neubauer, "Genetic design of analog IIR filters with variable time delays for optically controlled microwave signal processors," Evolutionary Computation, IEEE International Conference on, pp. 437 - 442, Apr. 1997.

[80].K. Hill, B. Malo, F. Bilodeau, D. Johnson, and J. Albert, "Bragg gratings fabricated in monomode photosensitive optical fiber by UV exposure through a phase mask," Applied Physics Lett., vol. 62, no. 10, pp. 1035-1037, Jul. 1993.

[81].K. O. Hill and G. Meltz, "Fiber Bragg grating technology fundamentals and overview," Invited paper, J. Lightwave Technol., vol. 15, no. 8, pp. 1263-1276, Aug. 1997.

[82].A. Othonos and K. Kalli, *Fiber Bragg gratings: Fundamentals and applications in telecommunications and sensing.* Artech House, Boston-London, 1999.

[83].R. Feced and M. N. Zervas, "Effects of random phase and amplitude errors in optical fiber Bragg gratings," J. Lightwave Technol., vol. 18, no. 1, pp. 90-101, Jan. 2000.

[84].George J. Meslener, "Chromatic dispersion induced distortion of modulated monochromatic light employing direct detection," IEEE Journal of Quantum Electronics, vol. QE-20, no. 10, pp. 1208-1216, Oct. 1984.

[85].U. Gliese, S. Norskov, and T. N. Nielsen, "Chromatic dispersion in fiber-optic microwave and millimeter-wave links," IEEE Trans. Microwave Theory and Technol., vol. 44, no. 10, pp. 1716-1724, Oct. 1996.

[86].J. L. Corral, J. Marti, J. M. Fuster and R. I. Laming, "Dispersion-induced bandwidth limitation of variable true time delay lines based on linearly chirped fiber gratings," IEE Electron. Lett., vol. 34, no. 2, pp. 209-211, Jan. 1998.

[87].Graham H. Smith, Dalma Novak, Zaheer Ahmed, "Overcoming chromatic-dispersion effects in fiber-wireless systems incorporating external modulators," IEEE Trans. Microwave Theory and Technol., vol. 45, no. 8, pp. 1410-1415, Aug. 1997.

[88].Ken-Ichi Kitayama, "Ultimate performance of optical DSB signal-based millimeter-wave fiber-radio system: effect of laser phase noise," J. Lightwave Technol., vol. 17, no. 10, pp. 1774-1781, Oct. 1999.

[89].V. Polo, F. Ramos, J. Marti, D. Moodie, and D. Wake, "Synthesis of photonic microwave filters based on external optical modulators and wide-band chirped fiber gratings," J. Lightwave Technol., vol. 18, no. 2, pp. 213-220, Feb. 2000.

[90].N. M. Litchinitser, B. J. Eggleton and D. B. Patterson, "Fiber Bragg gratings for dispersion compensation in transmission: theoretical model and design criteria for nearly ideal pulse recompression," J. Lightwave Technol., vol. 15, no. 8, pp. 1303-1313, Aug. 1997.

[91].B. Ortega, J. L. Cruz, J. Capmany, M. V. Andres, and D. Pastor, "Variable delay line for phased-array antenna based on a chirped fiber

grating," IEEE Trans. Microwave Theory and Technol., vol. 48, no. 8 , pp. 1352 -1360, Aug. 2000.

[92].Ken-ichi Kiyayama, Toshiaki Kuri, Kiyoshi Onohara, Tomotada Kamisaka and Kiyotaka Murashima, "Dispersion effects of FBG filter and optical SSB filtering in DWDM millimeter-wave fiber-radio systems," J. Lightwave Technol., vol. 208, no. 8, pp. 1397-1407, Aug. 2002.

[93].J. Mora, B. Ortega, J. L. Cruz, J. Capmany, D. Pastor, M. V. Andres, "White light sources filtered with fiber Bragg gratings for RF-photonics applications," Optics Communications, Elsevier Science, vol. 222, pp. 221-225, May. 2003.

[94].H. Zmuda, E. N. Toughlian, *Photonic Aspects of Modern Radar*. Artech House, Boston, MA, 1994.

[95].R. C. Hansen, *Phased Array Antennas*. John Wiley, 1997.

[96].Dennis T.K. Tong and Ming C. Wu, "Multiwavelength Optically Controlled Phased-Array Antennas," IEEE Trans. Microwave Theory and Technol., vol. 46, no. 1, pp. 108-115, Jan. 1998.

[97].H. L. Van Trees, *Optimum Array Processing*. Wiley, New York, 2002.

[98].Y. Liu, J. P. Yao and J. Yang, "Wideband true-time-delay unit for phased array antenna using discrete-chirped fiber Bragg grating prism," Optics Communications, Elsevier Science, vol. 207, pp. 177-187, Jun. 2002.

[99].J. P. Yao, J. Yang and Y. Liu, "Continuous true-time-delay beamforming employing a multiwavelength tunable fiber laser source," IEEE Photon. Technol. Lett., vol. 14, no.5, pp. 687 -689, May. 2002.

[100]. Ming C. Wu, D. T. K Tong, "Multiwavelength Optically Controlled Phased-Array Antennas," IEEE Trans. Microwave Theory and Technol, vol. 46, no. 1, pp. 108-115, Jan. 1998.

[101]. F. Coppinger, S. Yegnanarayanan, P. D. Trinh, and B. Jalali, "All-optical incoherent negative taps for photonics signal processing," Electron. Lett., vol. 33, pp. 973-975, May. 1997.

[102]. F. Coppinger, S. Yegnanarayanan, P. D. Trinh, and B. Jalali, "All-optical RF filter using amplitude inversion in a semiconductor optical amplifier," IEEE Trans. Microwave Theory and Technol., vol. 45, no. 8, pp. 1473-1477, Aug. 1997.

[103]. X. Wang, L. Y. Chan, etc., "All-optical incoherent negative tap fiber optic delay lines using injection-locked F-P laser diode," Proc. 1998, 11th annual meeting IEEE lasers Electro-optics Society, pp. 229-230, Dec. 1998.

[104]. Deming Liu, Jun Hong Ng, and Chao Lu, "Wavelength conversion based on cross-gain modulation of ASE spectrum of SOA," IEEE Photon. Technol. Lett., vol. 12, pp. 1222-1224, Sept. 2000.

[105]. S. Li, K. S. Chiang, W. A. Gambling, Y. Liu, L. Zhang, and I. Bennnion, "A novel tunable all-optical incoherent negative-tap fiber-optic transversal filter based on a DFB laser diode and fiber Bragg gratings," IEEE Photon. Technol. Lett., vol. 12, no. 9, pp. 1207-1209, Sept. 2000.

[106]. Y. Xiaoke, F. Wei, N. J. Hong, and Lu. Chao, "Tunable microwave filter design using wavelength conversion technique and high dispersion time delays," IEEE Photon. Technol. Lett., vol. 13, no.8, pp. 857 -859, Aug. 2001.

LIST OF ACRONYMS

A

AM	Amplitude Modulation
ASE	Amplified Spontaneous Emission
AWG	Arrayed Wave Guide

C

CFBG	Chirped Fiber Bragg Grating

D

DFA	Doped Fiber Amplifier
DSB	Double Side Band

E

EDFA	Erbium Doped Fiber Amplifier
EMI	Electromagnetic Interference
EOM	Electro-Optic Modulator

F

FBG	Fiber Bragg Grating
FIR	Finite Impulse Response
FSR	Free Spectral Range
FWHM	Full Width at Half Maximum

G

GA	Genetic Algorithm

I

IIR	Infinite Impulse Response
IM	Intensity Modulation

L

LD	Laser Diode
LED	Light Emission Diode
LMS	Least Mean Square
LSB	Lower Side Band

M

MA	Moving Average
MM	Minimum Maximum
MSW	Magneto Static Wave

O

OSA	Optical Spectrum Analyzer

P

PC	Polarization Controller
PD	Photodetector
PM	Phase Mask

R

RF	Radio Frequency

S

SAW	Surface Acoustic Wave

SDL Super-conducting Delay-Line
SOA Semiconductor Optical Amplifier
SSB Single Side Band

U

UFBG Uniform Fiber Bragg Grating
USR Upper Side Band
UV Ultraviolet

X

XGM Cross Gain Modulation